GEOSPHERE

GEOSPHERE, v. 18, no. 1

https://doi.org/10.1130/GES02385.1

10 figures; 1 table; 1 set of supplemental files

CORRESPONDENCE: ctrexler@usgs.gov

CITATION: Trexler, C.C., Cowgill, E., Niemi, N.A., Vasey, D.A., and Godoladze, T., 2022, Tectonostratigraphy and major structures of the Georgian Greater Caucasus: Implications for structural architecture, along-strike continuity, and orogen evolution: Geosphere, v. 18, no. 1, p. 211–240, https://doi.org/10.1130/GES02385.1.

Science Editor: Andrea Hampel Associate Editor: Jeff Lee

Received 11 December 2020 Revision received 20 July 2021 Accepted 26 August 2021

Published online 6 January 2022





This paper is published under the terms of the CC-BY-NC license.

© 2022 The Authors

Tectonostratigraphy and major structures of the Georgian Greater Caucasus: Implications for structural architecture, along-strike continuity, and orogen evolution

Charles C. Trexler^{1,*}, Eric Cowgill¹, Nathan A. Niemi², Dylan A. Vasey¹, and Tea Godoladze³

- ¹Department of Earth & Planetary Sciences, University of California, Davis, California 95616, USA
- ²Department of Earth & Environmental Sciences, University of Michigan, Ann Arbor, Michigan 48109, USA
- ³Institute of Earth Sciences & National Seismic Monitoring Center, Ilia State University, Tbilisi 0177, Georgia

ABSTRACT

Although the Greater Caucasus Mountains have played a central role in absorbing late Cenozoic convergence between the Arabian and Eurasian plates, the orogenic architecture and the ways in which it accommodates modern shortening remain debated. Here, we addressed this problem using geologic mapping along two transects across the southern half of the western Greater Caucasus to reveal a suite of regionally coherent stratigraphic packages that are juxtaposed across a series of thrust faults, which we call the North Georgia fault system. From south to north within this system, stratigraphically repeated ~5-10-km-thick thrust sheets show systematically increasing bedding dip angles (<30° in the south to subvertical in the core of the range). Likewise, exhumation depth increases toward the core of the range, based on low-temperature thermochronologic data and metamorphic grade of exposed rocks. In contrast, active shortening in the modern system is accommodated, at least in part, by thrust faults along the southern margin of the orogen. Facilitated by the North Georgia fault system, the western Greater Caucasus Mountains broadly behave as an in-sequence, southward-propagating imbricate thrust fan, with older faults within the range progressively abandoned and new structures forming to accommodate shortening as the thrust propagates southward. We suggest that the single-fault-centric "Main Caucasus thrust" paradigm is no longer appropriate, as it is a system of faults, the North Georgia fault system, that dominates the architecture of the western Greater Caucasus Mountains.

■ INTRODUCTION

The Greater Caucasus Mountains define the northern margin of the Arabia-Eurasia collision zone between the Black and Caspian Seas and formed

Charles C. Trexler https://orcid.org/0000-0001-5046-9729

as the result of Cenozoic structural inversion of a Mesozoic marine basin (Fig. 1A; Adamia et al., 2011a, 2011b; Banks et al., 1997; Dotduyev, 1986; Philip et al., 1989). However, the size and structure of the Mesozoic basin and the timing and mechanism of its closure are debated (e.g., Cowgill et al., 2016, 2018; Vincent et al., 2016, 2018). A central feature in this debate is an apparent contradiction in our understanding of orogenic architecture and active shortening from geodetic and regional tectonic studies.

Geodetic observations suggest that the majority of Arabia-Eurasia shortening at the latitude of the Greater Caucasus is being accommodated on structures within the Greater Caucasus Mountains (e.g., Philip et al., 1989; Jackson, 1992; Allen et al., 2004; Reilinger et al., 2006), which root into a shallowly north-dipping fault beneath the range (Sokhadze et al., 2018). Meanwhile, structural observations from the region suggest that faults within the core of the orogen are steeply dipping and thus are not favorably oriented to accommodate active tectonic shortening (e.g., Somin, 2000). In addition, these faults also appear to have relatively little horizontal displacement across them, calling into question whether they play a significant role in the modern orogen. In one end-member model, the Greater Caucasus Basin was a narrow continental rift, and likely floored by continental crust (e.g., Vincent et al., 2016, 2018). In the other, the basin was relatively wide and may have been underlain by oceanic or extensionally thinned continental crust (e.g., Cowgill et al., 2016, 2018). These two end-member models of orogen architecture make discrete predictions regarding where and how shortening is accommodated within the orogen. In the first, the rift inversion model, shortening is accommodated across subvertical structures and should be expressed by vertical exhumation and minimal horizontal shortening. In the second, the subduction/underthrusting to collision model, shortening is accommodated on more shallowly dipping structures on the flanks of the orogen, and expressions of orogenic growth should be primarily manifested in horizontal shortening, with minimal vertical exhumation. Additionally, this second model implies the existence of a tectonic suture within the orogen—a structure or set of structures that delineates the transition from the overriding plate to the underthrust plate.

The key to differentiating between these models lies in identifying and unraveling the kinematics of deformation across major faults within the orogen.

^{*}Present address: U.S. Geological Survey Earthquake Science Center, P.O. Box 158, Moffett Field, California 94035, USA

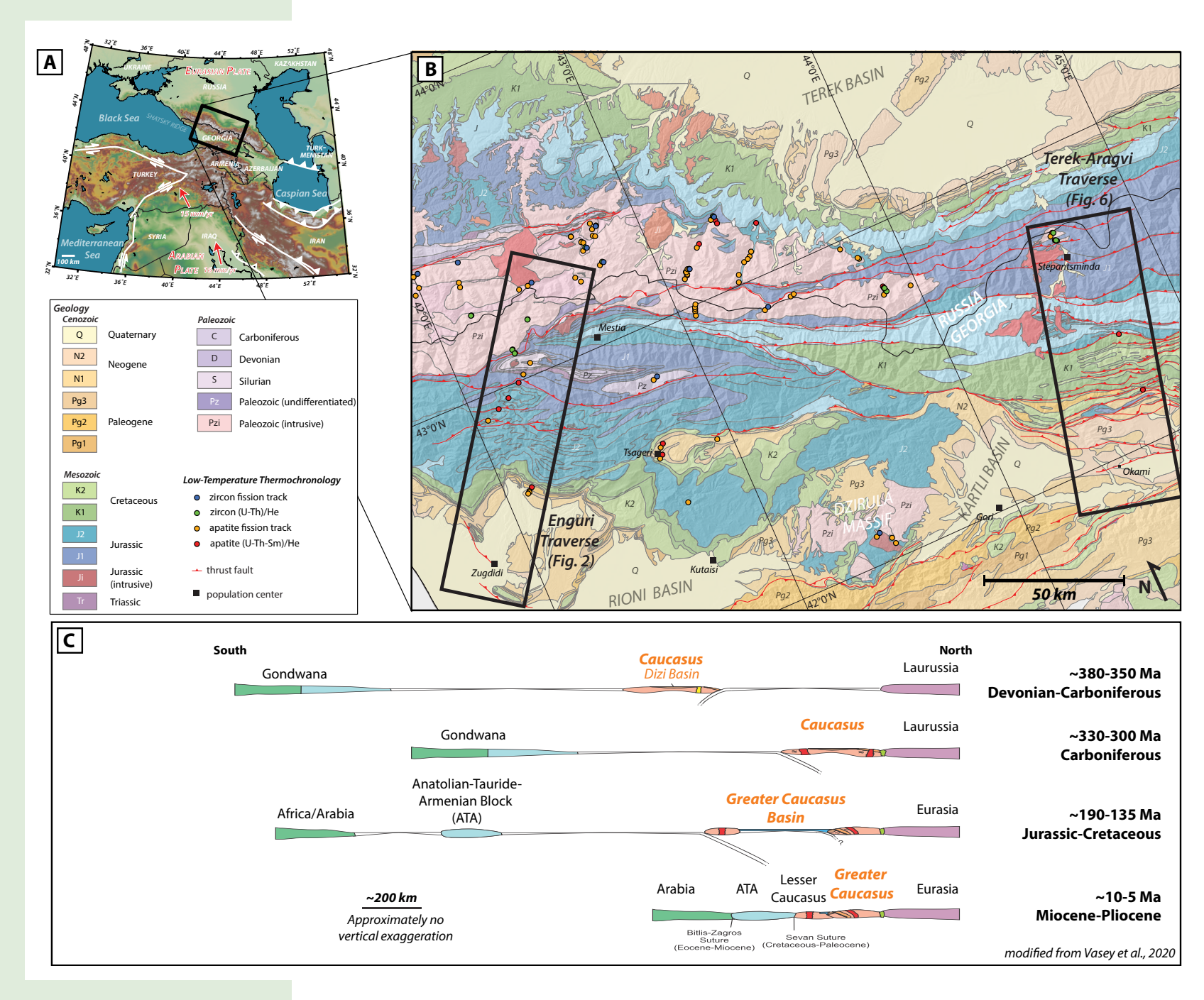


Figure 1. (A) Overview map of the Arabia-Eurasia collision zone, with the Greater Caucasus at the northern margin, modified from Forte (2012). (B) Compilation of 1:200,000 scale geologic mapping (Dzhanelidze and Kandelaki, 1957; Kandelaki, 1957; Zdilashavili, 1957: Gamkrelidze and Kakhazdze, 1959) and low-temperature thermochronology data (circles; Hess et al., 1993; Kral and Gurbanov, 1996; Avdeev, 2011; Avdeev and Niemi, 2011; Vincent et al., 2011) from the western Greater Caucasus. (C) Schematic cross sections illustrating the Phanerozoic tectonic evolution of the Greater Caucasus (orange block and text), modified from Vasey et al. (2020).

Until recently, relatively few regional-scale structural geology studies have been reported, in part due to limited access for political reasons prior to the last decade. As a result, few structural observations have been reported from the core of the range, leaving uncertainty in the locations and geometries of faults and folds.

A broad array of new data sets from the Greater Caucasus has been published in recent years, including low-temperature thermochronology to constrain exhumation timing and magnitude (e.g., Avdeev and Niemi, 2011; Vincent et al., 2011, 2020; Vasey et al., 2020), sediment provenance analysis to constrain paleogeography (e.g., Morton et al., 2003; Vincent et al., 2014; Cowgill et al., 2016; Tye et al., 2021), and investigation of geomorphic indices of uplift (e.g., Forte et al., 2014) and geodetic data (e.g., Reilinger et al., 2006; Kadirov et al., 2012; Sokhadze et al., 2018) to constrain modern deformation patterns. Structural and tectonic studies (e.g., Alania et al., 2020a, 2020b; Tibaldi et al., 2018, 2020; Vasey et al., 2020) are often localized and do not report regionally distributed structural data from the core of the range, which are critical for establishing a tectonic framework in which to interpret the new data sets in the context of active orogenic uplift and evolution.

Here, we present new field observations, stratigraphic and structural data, and a compilation of new and previously published low-temperature thermochronology analyses, which together further elucidate the structural architecture of the western Greater Caucasus. These data support a model of the orogen behaving as a growing imbricate fan, where shallowly dipping active structures define the leading edge of the mountain belt as back-rotated, more steeply dipping structures are abandoned in the interior of the range, rather than through inversion of rift-related high-angle faults. This model provides an internally consistent framework for integrating geodetic and structural observations in the orogen. Additionally, by highlighting a network of multiple significant structures within the orogen, this model of orogenic architecture provides a productive framework for further investigations into the tectonic setting and history of the western Greater Caucasus.

■ BACKGROUND

Geologic Setting

The Arabia-Eurasia plate collision extends from the eastern Mediterranean in the west to Afghanistan in the east (Fig. 1A). The Caucasus region, in the center of the Arabia-Eurasia collision zone, is bounded by the Black Sea to the west and the Caspian Sea to the east. The region extends from southern Russia at its northern edge, across the nations of Georgia, Azerbaijan, and Armenia in the center, to the Pontide, Lesser Caucasus, and Alborz Mountains along its southern margin in Turkey, Azerbaijan, and Iran, respectively.

The Paleozoic history of the Caucasus region is recorded in sparse exposures of metasedimentary and crystalline rocks in the core of the Greater Caucasus, primarily in the half of the orogen west of ~45°E (Fig. 1B). Ordovician- to

Carboniferous-age crystalline basement, a combination of plutonic and metamorphic rocks (Nalivkin, 1973; Vasey et al., 2020), is commonly associated with the Scythian Platform, a complexly deformed zone on the southern edge of the East European craton that has been interpreted as a complex orogenic belt and/or a Paleozoic island-arc system (Natal'in and Sengör, 2005; Nikishin et al., 2011). The Dzirula Massif, a block of metamorphic and igneous basement located at the southern margin of the western Greater Caucasus in central Georgia (Fig. 1B), is widely considered to be a fragment of the crystalline basement core (Zakariadze et al., 2007), though new detrital zircon analyses suggest these crystalline blocks may in fact be distinct in origin (Tye et al., 2021). Metasedimentary rocks of similar age to the crystalline core, known as the Dizi Series, are exposed in a limited area of the western Greater Caucasus, primarily in the Svaneti region of Georgia. Interpretation of detrital zircon analyses suggested that the Dizi Series may represent a back-arc basin adjacent to a proto-Greater Caucasus island arc associated with south-directed subduction prior to accretion onto the Laurentian margin during the Carboniferous (Fig. 1C; Vasey et al., 2020).

The majority of exposed strata within the Greater Caucasus were deposited during the Mesozoic, in a depocenter broadly referred to as the Greater Caucasus Basin (Dotduyev, 1986; Philip et al., 1989; Banks et al., 1997; Adamia et al., 2011b). Jurassic- to Cretaceous-age marine sedimentary rocks, primarily slate/shale and fine sandstone turbidites, dominate much of the Caucasus Basin section (Dzhanelidze and Kandelaki, 1957; Kandelaki and Kakhazdze, 1957; Gamkrelidze and Kakhazdze, 1959; Gubkina and Ermakov, 1989; Adamia et al., 2011b). In the western Greater Caucasus, the southern part of the range contains extensive deposits of volcanic breccia and volcaniclastic rock, along with shallow-marine and terrestrial sedimentary rocks overlain by Cretaceous limestone (Dzhanelidze and Kandelaki, 1957; Gamkrelidze and Kakhazdze, 1959; Adamia et al., 2011b). Stratigraphic and geochemical analyses of the Mesozoic section suggest the Greater Caucasus Basin likely formed as a back-arc rift basin related to north-directed subduction of the Tethys Ocean basin beneath the Late Jurassic-Eocene-age Lesser Caucasus/Pontide arc to the south (Yilmaz et al., 2000; McCann et al., 2010; Mosar et al., 2010). This arc is now exposed as the Achara/Trialet and Lesser Caucasus Mountains, which demarcate the southern limit of the Caucasus region. Along with the Shatsky Ridge in the eastern Black Sea, the Dzirula Massif (see previous paragraph) may also define the southern margin of the Mesozoic Greater Caucasus Basin (Banks et al., 1997; Vincent et al., 2014; Adamia et al., 2017). The tectonic setting of the Greater Caucasus Basin—the scale and geometry of the basin, and whether it was floored by oceanic or continental crust—is still debated (e.g., Cowgill et al., 2016, 2018; Vincent et al., 2016, 2018).

Cenozoic rocks in the western Greater Caucasus record the closure of the Greater Caucasus Basin and growth of the modern Greater Caucasus Mountains. Paleogene and Neogene strata in sedimentary basins along the southern flank of the Greater Caucasus typically consist of clastic marine to terrestrial sedimentary rocks, reflecting a generally shallowing depositional setting through time. These basins include the wedge-top Rioni, Kartli, and Alazani

basins in the western and central Greater Caucasus, and the flexural foreland Kura basin in the east (e.g., Banks et al., 1997; Forte et al., 2013). South-directed fold-and-thrust belts within these flanking basins expose Cretaceous- to Neogene-age strata. Surface geology and seismic-reflection data suggest that the fold-and-thrust belts have a thin-skinned structural geometry (e.g., Banks et al., 1997; Forte et al., 2010; Alania et al., 2017; Adamia et al., 2017; Tibaldi et al., 2017b) and are presently active (e.g., Banks et al., 1997; Forte et al., 2013; Trexler et al., 2020; Tibaldi et al., 2018).

Modern Tectonic Setting

Results of low-temperature thermochronology studies in the western Greater Caucasus orogen suggest that exhumation of the range began by ca. 35 Ma (Vincent et al., 2007, 2011; Avdeev and Niemi, 2011). This timing is consistent with estimated subduction initiation of the Greater Caucasus back-arc basin (Zonenshain and Le Pichon, 1986; Natal'in and Sengör, 2005; Avdeev and Niemi, 2011), when closure of relict ocean basins in the Caucasus and East Anatolian Plateau is argued to have absorbed continental convergence (Cowgill et al., 2016). Cooling rates increased dramatically ca. 5 Ma (Avdeev and Niemi, 2011), an event hypothesized by proponents of the collision model of orogen growth to correspond to the final, "hard" continent-continent collision associated with the subduction of the last remnants of the Greater Caucasus ocean basin at this longitude and resulting in a structural reorganization throughout the Arabia-Eurasia collision zone (Avdeev and Niemi, 2011; Cowgill et al., 2016). Prior work on the structural architecture of the Greater Caucasus assumed that the locus of Cenozoic shortening was located along a dominant, deeply rooted structural system called the Main Caucasus thrust, which was variably placed at the base of the crystalline basement in the core of the range, within the marine sedimentary package of the Caucasus Basin to the south, or at the southern topographic range front (Saintot et al., 2006; Mosar et al., 2010; e.g., Adamia et al., 2011b). Neotectonic investigations of active fold-and-thrust belts in the eastern (Forte et al., 2010, 2013; Mosar et al., 2010; Kadirov et al., 2012) and western (Banks et al., 1997; Alania et al., 2017; Tsereteli et al., 2016; Tibaldi et al., 2017a) Greater Caucasus suggest that the presently defined Main Caucasus thrust (e.g., Vasey et al., 2020) may represent a significant lithotectonic boundary within the Caucasus orogen, but it is unlikely to be the trace of the active or dominant orogenic structure at the surface.

METHODS

To directly test these two models of orogen evolution, we conducted 1:100,000 scale geologic mapping along two transects across the Greater Caucasus. We combined the results of our mapping with provenance analyses and low-temperature thermochronology to characterize the first-order structure of the western Greater Caucasus in the Republic of Georgia.

Mapping

We conducted 1:100,000 scale geologic mapping along two transects roughly perpendicular to the strike of the range: the Enguri traverse, at approximately azimuth 035°, and the Terek-Aragvi traverse, at approximately azimuth 0° (Fig. 1B). We focused our mapping within the Greater Caucasus Basin zone of the Greater Caucasus, bounded by the crystalline core of the range to the north and the foreland fold-and-thrust belt to the south. We used published 1:200,000 scale geologic maps to extrapolate mapping along strike between our two traverses.

We collected field data primarily by foot along roads and trails along (1) the Enguri River between the towns of Zugdidi and Mestia in western Georgia, which we refer to as the Enguri traverse, and (2) along Highway E117, a major trans-Caucasus highway that follows the north-draining Terek River and south-draining Aragvi River between the Russian border north of Stepantsminda and the town of Jinvali in central Georgia, which we refer to as the Terek-Aragvi traverse (Fig. 1B). Exposure limitations, including steep topography with dense vegetation below tree line, restricted mapping to zones along river valleys and road cuts. Along the mapping transects, rock exposures were discontinuous, with ~5-30-m-long exposures separated by ~200-1000-m-long covered intervals. To augment existing data most efficiently, we focused our field efforts on collecting structural observations, particularly bedding orientation, stratigraphic facing direction, and the locations of major contacts and structures. We combined the results of our field mapping with existing published maps (Dzhanelidze and Kandelaki, 1957; Kandelaki, 1957; Zdilashavili, 1957; Gamkrelidze, 1958; Gamkrelidze and Kakhazdze, 1959; Gubkina and Ermakov, 1989), which we reinterpreted in the context of our structural and lithologic observations.

Definition of Georgian Tectonostratigraphy

Existing geologic maps for our study area (Dzhanelidze and Kandelaki, 1957; Kandelaki, 1957; Zdilashavili, 1957; Gamkrelidze, 1958; Gamkrelidze and Kakhazdze, 1959; Gubkina and Ermakov, 1989) have limited available stratigraphic descriptions and are at a smaller scale than our field mapping, precluding their use in delineating local unit descriptions and identifications. We therefore defined a suite of tectonostratigraphic units along each field traverse based on rock type, internal stratigraphic sequence, degree of metamorphism, and structural orientation and style. Each domain was named for the fault that bounded it to the south.

Exposures of the bounding faults were sparse, but their locations and dip directions could be inferred using structural and stratigraphic information from exposures flanking the structures, with evidence of faulting based on features such as an abrupt change in metamorphic grade or the truncation of stratigraphic facing direction and bedding. Correlation of the tectonostratigraphic domains along strike was, at least in some cases, viable and yielded further

insight into the stratigraphic architecture of the Greater Caucasus Basin and the structural geometry of the fault system that bounds the southern margin of the western Greater Caucasus.

Within the tectonostratigraphic domains, we defined individual map units based on rock type using field descriptions of stratigraphy and petrologic observations made both in outcrop and from hand samples. To further assess unit correlation, we augmented these data using thin-section petrography, with particular focus on the presence/absence of specific grain types.

To estimate stratigraphic thickness, we used calculations based on bedding dips and the locations of mapped/inferred contacts between tectonostratigraphic units along our traverses under the assumption that unit thicknesses were uniform along and across strike, although we acknowledge that this is an oversimplification. We report the depositional ages of collocated units on published 1:200,000 scale maps (Dzhanelidze and Kandelaki, 1957; Kandelaki, 1957; Zdilashavili, 1957; Gamkrelidze, 1958; Gamkrelidze and Kakhazdze, 1959; Gubkina and Ermakov, 1989). Published maps relied on biostratigraphic data to support age determinations; however, details on these ages were not always reported, and the sources of these data were difficult to validate (and thus recalibrate) in light of evolving relationships between biostratigraphic and absolute age values. Perhaps more importantly, the stratigraphic and spatial resolution of these biostratigraphic age determinations has not been clearly established. As such, the reliability of these age determinizations is unclear. Detrital zircon studies within the Greater Caucasus (Vincent et al., 2013; Cowgill et al., 2016; Tye et al., 2021) have yielded maximum depositional ages for units that, in most cases, agree with published biostratigraphic ages, but the geographic distribution of these provenance studies is limited, and in some cases maximum depositional ages are considerably older than the reported ages (Vasey et al., 2020).

Geochemical and Geochronological Analyses

The ⁴He for apatite helium (U-Th-Sm)/He thermochronometry was measured at the University of Michigan Thermochronology Laboratory using an Australian Scientific Instruments Alphachron helium instrument according to analytical procedures outlined in the appendix of Niemi and Clark (2018). We augmented these results with four previously unpublished apatite fission-track thermochronometry analyses (Avdeev, 2011). In addition, we compiled published low-temperature thermochronometry data from the Greater Caucasus (Fig. 2; Supplemental Table S5¹; Hess et al., 1993; Kral and Gurbanov, 1996; Avdeev, 2011; Avdeev and Niemi, 2011; Vincent et al., 2011, 2020; Vasey et al., 2020).

We performed zircon U-Pb analyses on one sedimentary sample from the Enguri traverse to provide age control and verify the age spectra previously reported for a sample (SWGC) from Cowgill et al. (2016). We present the resulting

age distribution using kernel density estimation generated by the DensityPlotter software (Fig. 2; Fig. S1; Vermeesch, 2012). We also conducted electron backscatter diffraction (EBSD) analysis on a single sample to investigate the structural fabrics in the highest metamorphic grade along the Enguri traverse.

We used whole-rock major- and trace-element geochemistry to assess the petrogenesis and tectonic setting of magmatic rocks within the western Greater Caucasus. Given that these rocks are typically interpreted to have been deposited/emplaced in the Caucasus Basin continental back-arc (Saintot et al., 2006; e.g., Adamia et al., 2011a; Vincent et al., 2016), where signatures range from island-arc basalt (IAB) to normal mid-ocean-ridge basalt (N-MORB) (e.g., Saunders and Tarney, 1984; Pearce and Stern, 2006), we compared trace-element signatures from our samples with N-MORB and IAB (e.g., Sun and McDonough, 1989; Kelemen et al., 2003) signatures. We present these data using the Th-3Tb-2Ta ternary diagram of Cabanis and Thieblemont (1988), a rare earth element (REE) plot normalized to primitive mantle values of McDonough and Sun (1995), and an incompatible trace-element diagram normalized to primitive mantle values of Sun and McDonough (1989). Additional details for all analytical methods are available in the Supplemental Material (see footnote 1).

■ ENGURI TRAVERSE RESULTS (WESTERN GREATER CAUCASUS)

In the westernmost Greater Caucasus, we mapped along the Nakra and Enguri Rivers between the town of Mestia (43.044°N, 42.724°E) in the north, near both the topographic divide of the range and the Georgia-Russia border, and the city of Zugdidi (42.509°N, 41.867°E), ~100 km to the southwest, located near the southern foreland basin and ~25 km inland from the eastern coast of the Black Sea (Fig. 2). Along this traverse, we defined five distinct tectonostratigraphic domains, and within each domain, we labeled the individual map units using abbreviations for the traverse, the domain name, and the lithology of each tectonostratigraphic unit.

Enguri Traverse Tectonostratigraphic Units and Their Bounding Structures

From north to south, the five domains along the Enguri traverse (E) are the Ushba (u), Dizi (d), Khaishi (k), Idliani (i), and Jvari (j) domains (Figs. 2 and 3). Four rock types comprise these domains: crystalline basement (x); clastic sedimentary rocks dominated by interlayered sandstone and mudstone (s); intrusive, volcanic, and volcaniclastic rocks (v); and limestone (Is). In cases where the same rock type occurred more than once within a single tectonostratigraphic domain, we numbered the units sequentially from oldest to youngest. In sum, we defined a total of nine discrete map units along this traverse. The Ushba domain contains exclusively crystalline basement, unit E-ux. The Dizi domain is composed of two distinct packages of metasedimentary rocks (E-ds1, E-ds2). The Khaishi domain contains both sedimentary and

¹Supplemental Material. Structural orientation data and raw data from geochemical and thermochronological analyses. Please visit https://doi.org/10.1130/GEOS.S.16834624 to access the supplemental material, and contact editing@geosociety.org with any questions.

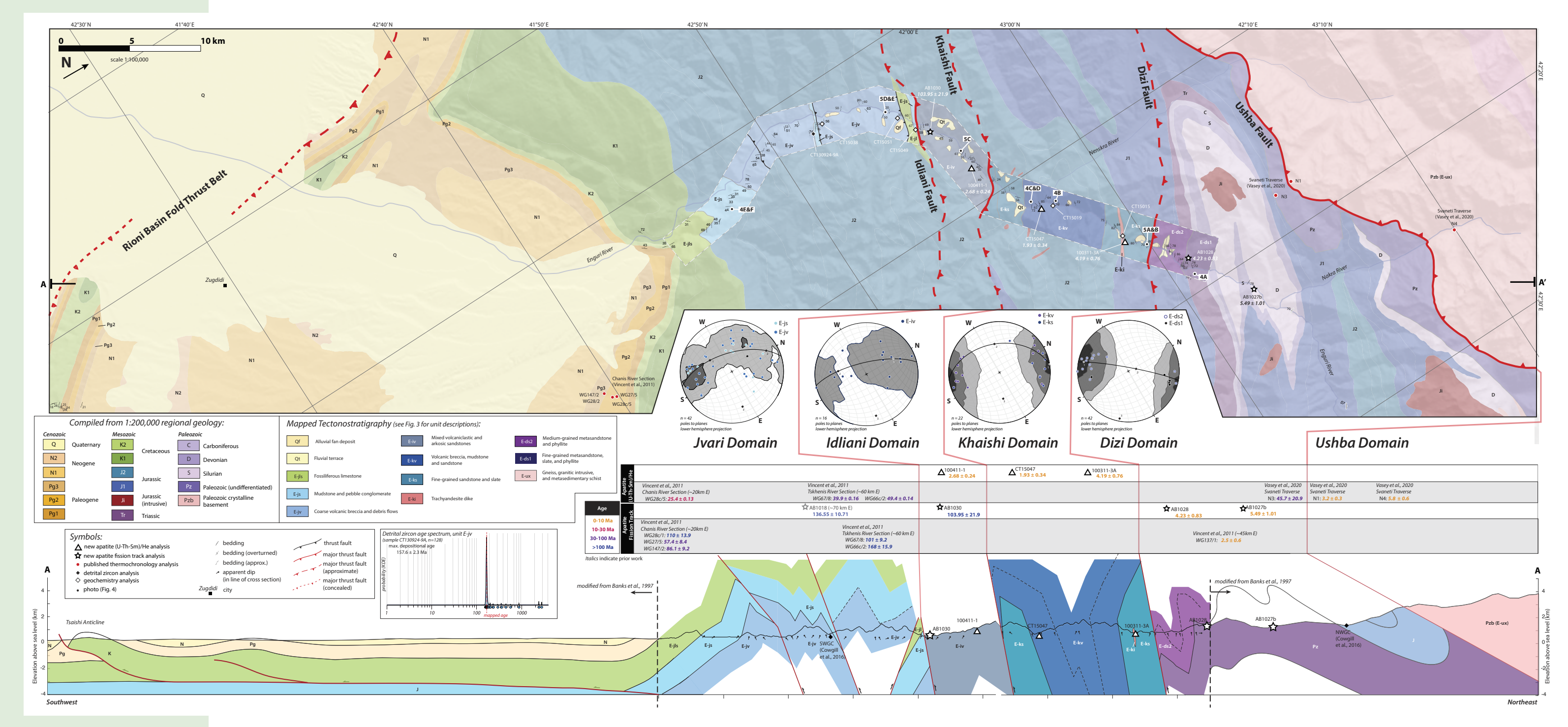
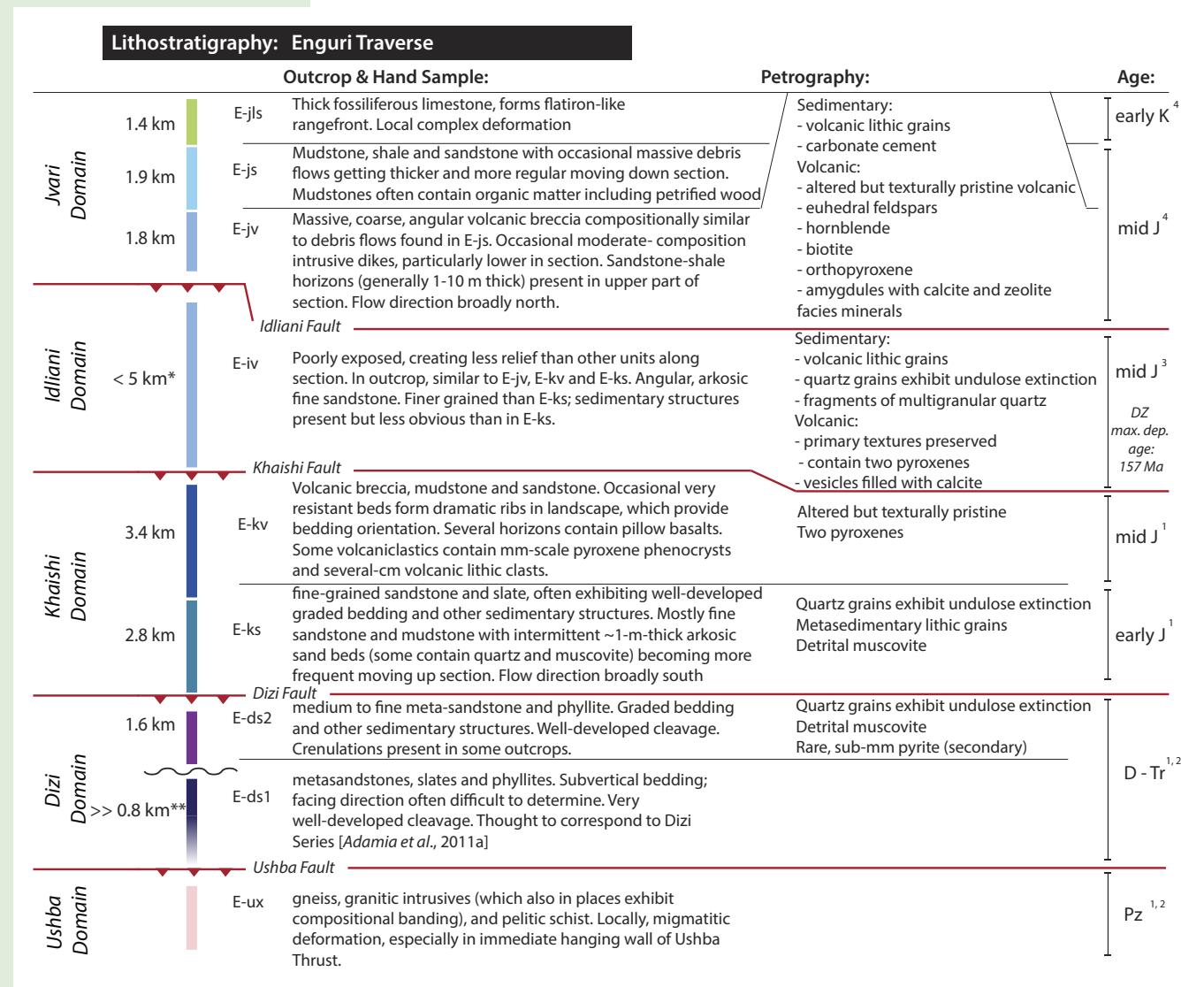


Figure 2. Geologic map of the Enguri traverse, western Greater Caucasus (long dimension 108 cm). Bold band in center outlined by white dashed line delineates our 1:100,000 mapping transect. Base map was compiled from 1:200,000 geologic maps (Dzhanelidze and Kandelaki, 1957; Kandelaki, 1957; Kandelaki, 1957; Gamkrelidze and Kakhazdze, 1959). Cross section was compiled from field data, 1:200,000 geologic maps (Dzhanelidze and Kandelaki, 1957; Gamkrelidze and Kakhazdze, 1959), and work by Banks et al. (1997) and Tibaldi et al. (2017b). Stereograms show poles to bedding planes in an equal-area projection and use a Kamb contour with an interval of 5. Apatite (U-Th-Sm)/He ages from Chanis and Tskhenis River sections (Vincent et al., 2011) appear to be averages of multiple multigrain aliquots of detrital samples and thus do not likely reflect geologically meaningful events (see text for discussion). Detrital zircon age spectrum for sample CT13094–9A is reported as a kernel density estimate (KDE, colored peaks) with ages of individual grains noted by blue circles beneath the plot. Age determinations are from U-Pb analysis of detrital zircon grains. See Supplemental Table S4 (text footnote 1) for detrital zircon U-Pb analysis results.



^{*} maximum estimated thickness, based on mapped exposure and bedding orientation. Internal deformation is significant, and actual thickness may be much less. ** minimum estimated thickness, based on mapped exposure and bedding orientation. Mapping extent limited by landslides and poor exposure; actual thickness may be significantly larger

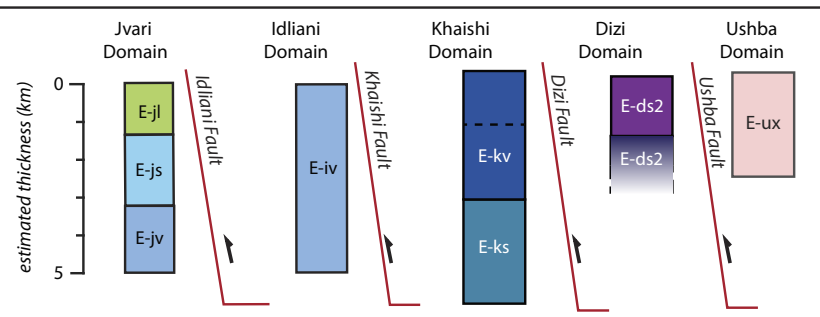


Figure 3. Tectonostratigraphic column for units in the Enguri traverse. Unit descriptions were compiled from outcrops, hand samples, and thin sections. Unit thicknesses were estimated based on mapping and structural data. References for mapped age: 1 - Gamkrelidze and Kakhazdze (1959); 2 - Vasey et al. (2020); 3 -Dzhanelidze and Kandelaki (1957); 4-Kandelaki (1957). K-Cretaceous; J-Jurassic; Tr-Triassic; Pz-Paleozoic; DZ-detrital zircon.

volcaniclastic strata (E-ks, E-kv). The Idliani domain contains a single unit of mixed volcaniclastic rocks (E-iv). The Jvari domain is the most diverse, containing clastic, volcaniclastic, and carbonate strata (E-js, E-jv, E-jls) (Figs. 2 and 3).

Although bedding dip angles were observed to be variable along the traverse, the strike direction was remarkably consistent and only varied by $\pm \sim 20^{\circ}$ from the average (stereograms, Fig. 2). Between the northern and southern ends of the traverse, measured average bedding strike rotated $\sim 20^{\circ}$ clockwise, from $\sim 280^{\circ} - 290^{\circ}$ in the north to $\sim 300^{\circ} - 310^{\circ}$ in the south.

Ushba Domain and Northern Flank

The Ushba domain is composed of crystalline basement, unit E-ux, and overlying sedimentary rocks beyond the northern extent of the mapping traverse (Fig. 1). In the map area, the crystalline basement primarily consists of amphibolite-facies metasedimentary and granitoid plutonic rocks that in places exhibit compositional banding (Fig. 3; Vasey et al., 2020), and localized zones of migmatite are present particularly in the immediate hanging wall of Ushba fault.

North of the map area, published maps show a gently north-dipping homocline that exposes a nearly complete stratigraphic section extending from crystalline basement in the core of the range up through Mesozoic marine basin sedimentary units and into Cenozoic synorogenic sedimentary units deposited on the flank of the growing orogen (Potapenko, 1964; Adamia et al., 2011b). No active structures have been mapped on the northern flank of the western Greater Caucasus (Potapenko, 1964).

Ushba Fault

The southern margin of the Ushba domain is defined by the north-dipping Ushba fault, which juxtaposes the crystalline basement in the core of the range in the hanging wall against Paleozoic and Mesozoic metasedimentary and sedimentary rocks in the footwall. The surface trace of this structure on published maps (Gamkrelidze and Kakhazdze, 1959), along with field observations, suggests this structure dips north at relatively low angle (~30°). This structure has been identified as the Main Caucasus thrust in this part of the range (e.g., Somin, 2011; Vasey et al., 2020). Low-temperature thermochronology data from this domain record Cenozoic zircon (U-Th)/He ages in both the hanging wall and footwall of this fault, suggesting that while it may accommodate some portion of Cenozoic exhumation within the range, some additional component of that exhumation must be accommodated on other structures to the south (Vasey et al., 2020).

Dizi Domain: Fine-Grained Marine Metasedimentary Rocks

Valley-bottom exposures are poor south of the contact with crystalline basement due to glacial deposits, vegetation, and mass wasting, obscuring

units in the footwall of the Ushba fault. Published maps show Jurassic to Cretaceous rocks in the footwall beneath the Ushba fault (Gamkrelidze and Kakhazdze, 1959), but we were unable to conclusively document outcrops of these units in the field. The first well-exposed unit to the south of the Ushba domain is the Dizi series, which defines the northern end of our mapping transect. Two units comprise the Dizi domain along the traverse, which we refer to here as E-ds1 and E-ds2.

Unit E-ds1 contains alternating beds of fine-grained metasandstone, slate, and phyllite. The contact between unit E-ds1 and unit E-ux is not well exposed, but it is shown as depositional on prior maps (Gamkrelidze and Kakhazdze, 1959). Sedimentary structures are not generally apparent, and unit facing direction is difficult to determine. Cleavage is well developed and easier to identify in outcrop than are bedding planes. The phyllite-grade metamorphism of unit E-ds1 is the highest grade exposed within the Enguri mapping traverse, outside of the gneissic textures exposed in crystalline basement to the north (Fig. 3). Compositional layering (presumed to be bedding) within E-ds1 is consistently steeply (~60°–80°) north-dipping layering (Table S1). Intersection angles between cleavage and compositional layering indicate alternating upright and overturned beds, suggesting isoclinal folding, but fold hinges are rarely exposed.

Unit E-ds2 stratigraphically overlies unit E-ds1, and it is composed of medium- to fine-grained metasandstone, slate, and phyllite. We did not directly document the contact relationship between these units, which prior mapping suggested is an angular unconformity (Gamkrelidze and Kakhazdze, 1959). Unit E-ds2 is differentiated from E-ds1 by its less prominent cleavage, by its increased proportion of psammitic to phyllitic textures, and by the increased presence of sedimentary structures, including graded bedding and scour marks. Unit E-ds2 exhibits moderately developed axial planar cleavage, more steeply dipping than upright bedding, and crenulation cleavage is present in some outcrops (Table S1).

Bedding within E-ds2 is consistently steeply (>60°) north-dipping bedding, and exposures show alternating stratigraphic facing direction, as indicated by sedimentary structures and cleavage-bedding intersection angles. Fold hinges are rarely exposed, but where found, they exhibit well-developed axial planar cleavage that is oriented subparallel to bedding throughout the surrounding unit.

Dizi Fault

The inferred Dizi fault separates unit E-ds2 to the north from unit E-ks to the south. This structure is inferred based upon an abrupt change in metamorphic grade and grain size (see description of units to south in following sections) and a juxtaposition of bedding attitudes across the contact. Specifically, north of the contact, stratigraphically upright beds in unit E-ds2 dip >~70°N, whereas to the south, stratigraphically upright beds in unit E-ks dip south and project updip directly into unit E-ds2. The fault is inferred to be subvertical or steeply north dipping, based upon the map trace and orientation of surrounding bedding.

Khaishi Domain: Mixed Marine Sedimentary Rocks and Volcanic and Volcaniclastic Deposits

The Khaishi domain is primarily composed of metasandstone and slate, which are generally coarser grained and of lower metamorphic grade than the Dizi domain to the north. Sedimentary structures are apparent in sandstone-bearing intervals, providing depositional facing and paleoflow directions. We subdivided the Khaishi domain into two major units, the stratigraphically lower E-ks and the stratigraphically higher E-kv units.

Unit E-ks is primarily composed of well-bedded, fine-grained sandstone and slate that commonly exhibit ~1- to 10-cm-scale graded bedding, scour marks, and load structures (Fig. 3). Paleocurrent directions are broadly south directed, based on outcrop exposures of cross-beds and scour marks (Fig. 4A). Nearly all bedding orientations are steeply inclined, and pervasive isoclinal folding is inferred based on abrupt changes in stratigraphic facing direction, as indicated by sedimentary structures, with steep dips to the north in both upright and overturned beds. Fold hinges are generally not exposed. Cleavage is present but poorly developed. Rocks within unit E-ks were subjected to low-grade regional metamorphism and do not contain evidence of recrystallization.

Along the mapping transect, unit E-ks is intruded by a trachyandesite dike (mapped as E-ki (Figs. 2 and 5) that is several meters thick and enveloped by a contact metamorphic aureole in the surrounding sedimentary rock. Both the sedimentary host rock and the dike are reported to be Early Jurassic in age (Gamkrelidze and Kakhazdze, 1959).

Unit E-kv conformably overlies unit E-ks and contains an assortment of volcanic breccia, mudrock, and sandstone. Resistant beds of volcanic breccia locally define prominent topographic ribs that are generally several tens of meters thick and typically provide the most robust bedding orientation information within this unit (Fig. 4B). The breccia deposits are matrix supported and contain blocks up to ~20 cm in diameter that are mafic to intermediate in composition. Several of the breccia horizons also contain several-meter-thick flows of pillow lava with individual pillows generally <1 m in diameter. In thin section, unit E-kv contains both orthopyroxene and clinopyroxene and largely remains texturally pristine (Fig. S1D), although the secondary growth of calcite and zeolite-facies minerals is also evident. This unit is reported to be Jurassic in age (Gamkrelidze and Kakhazdze, 1959). Bedding within E-kv is steeply north dipping and isoclinally folded, as indicated by bedding and stratigraphic facing directions inferred from sedimentary structures preserved within interbedded sedimentary units (e.g., Fig. 4C).

Khaishi Fault

The Khaishi fault defines the southern limit of the Khaishi domain, where it juxtaposes unit E-ks to the north against E-iv to the south. The structure was not observed directly in the field and was inferred based on changes in rock type and bedding orientations. The fault dips northward, constrained by the

orientation of the contact across topography and consistent with the orientation of both footwall and hanging-wall stratigraphy. South of the Khaishi fault, bedrock exposure is poor, bedding dips are more variable than north of the fault, and average topographic steepness is markedly reduced as compared to the northern tectonostratigraphic domains.

Idliani Domain: Mixed Volcaniclastic and Marine Sedimentary Rocks

South of the Khaishi fault, the Idliani domain is dominated by poorly exposed volcaniclastic and sedimentary rocks that we define as unit E-iv. Sedimentary horizons are generally fine-grained sandstone, with sedimentary structures such as graded beds, cross-beds, load structures, and scours present but less obvious than in units E-ks and E-ds2. Volcanic clasts in thin section preserve primary textures (Fig. S1) and contain both orthopyroxene and clinopyroxene.

Bedding within the Idliani domain generally dips shallowly to moderately (~25°–60°) southward. Poles to bedding planes define a crude northeast-southwest–striking girdle, indicating relatively cylindrical folding, and a structural geometry that is distinct from the isoclinal folding that dominates in northern domains (Fig. 2). Topographic relief throughout the region that is underlain by unit E-iv is lower than that preserved in regions underlain by other units along the Enguri traverse. Several outcrops expose breccia and cataclasite, but the poor exposure limited further evaluation of the lithology and internal structure of this unit.

Idliani Fault

The southern boundary of the Idliani domain is defined by the Idliani fault, an inferred structure that juxtaposes unit E-iv in the north against units E-jls and E-js of the Jvari domain to the south. The Idliani fault is the most poorly constrained fault along the traverse. Orientation data of the fault within the Idliani domain (inferred hanging wall) are limited and thus provide little constraint on its orientation. We inferred a northward dip based upon the "rule of V's" and map patterns on published geologic maps where the fault crosses the Enguri River valley (Gamkrelidze and Kakhazdze, 1959). This fault is associated with a change in topographic relief and lithology, with more rugged topography to the south as compared to subdued topography and poor exposures characteristic of E-iv to the north.

Jvari Domain: Volcaniclastic Rocks and Volcanic Breccias, and Shallow-Marine and Terrestrial Sedimentary Rocks

In contrast to the fine-grained, distal sedimentary units prevalent in the domains north of the Idliani fault, rocks of the Jvari domain to the south are

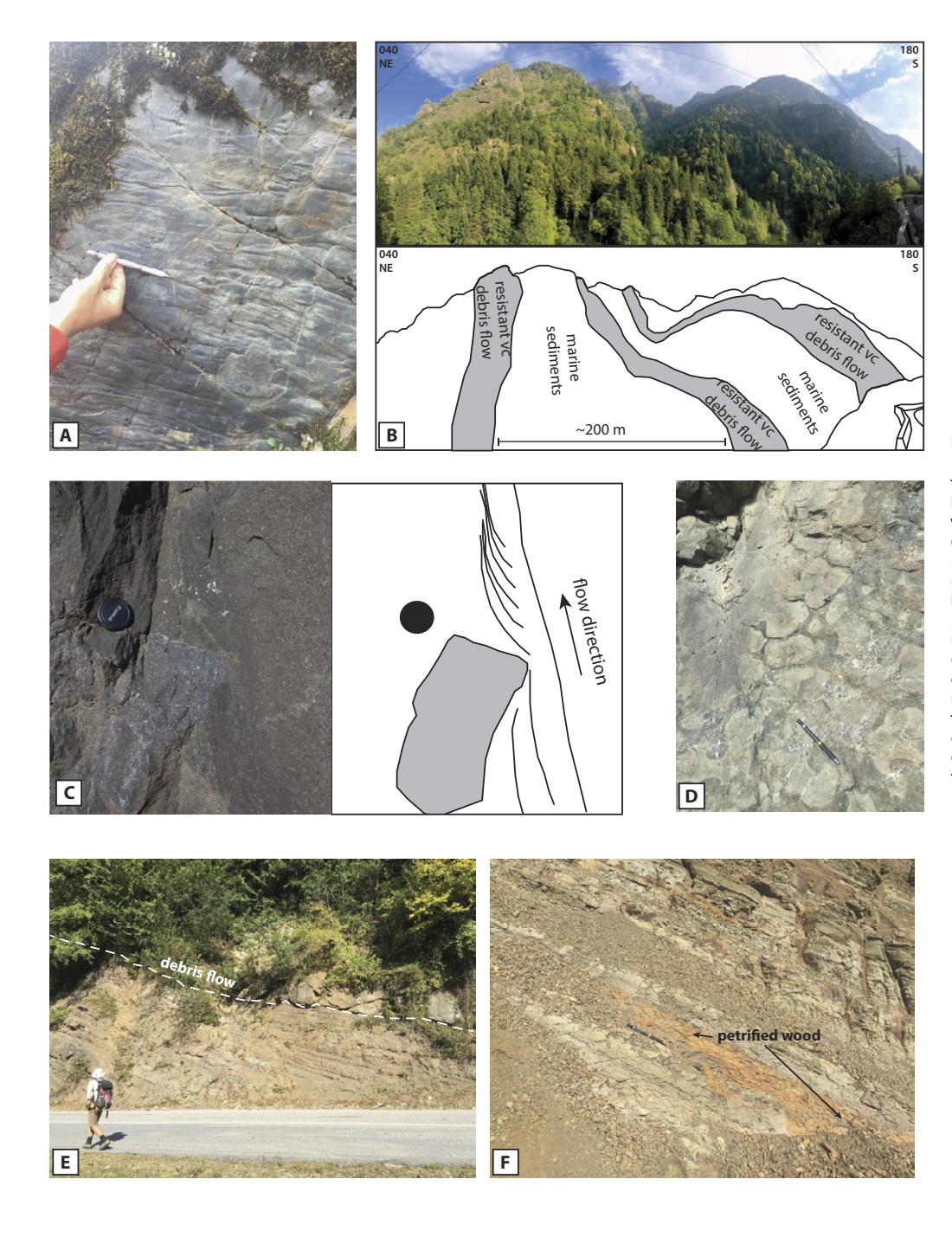


Figure 4. Field photographs. (A) Scour casts on a bedding plane in unit E-ds1. (B) Panorama (photo top and sketch representation bottom) looking SE at topographic expression of resistant volcaniclastic beds within unit E-kv. vc-volcaniclastic. (C) Within unit E-kv, volcaniclastic blocks are commonly incorporated into marine sediments at the bases of those horizons. Facing NW. (D) E-kv volcaniclastic package includes pillow lavas from 10 cm scale (shown here) to meter scale. Facing WNW. (E) At the southern end of the Enguri traverse, unit E-js contains deltaic and fluvial deposits interbedded with resistant volcaniclastic debris flows (visible at top of road cut). Facing N. (F) Fluvial and deltaic deposits of E-js contain ~10 cm pieces of charcoal and petrified wood (center of image, pencil for scale). Facing N.

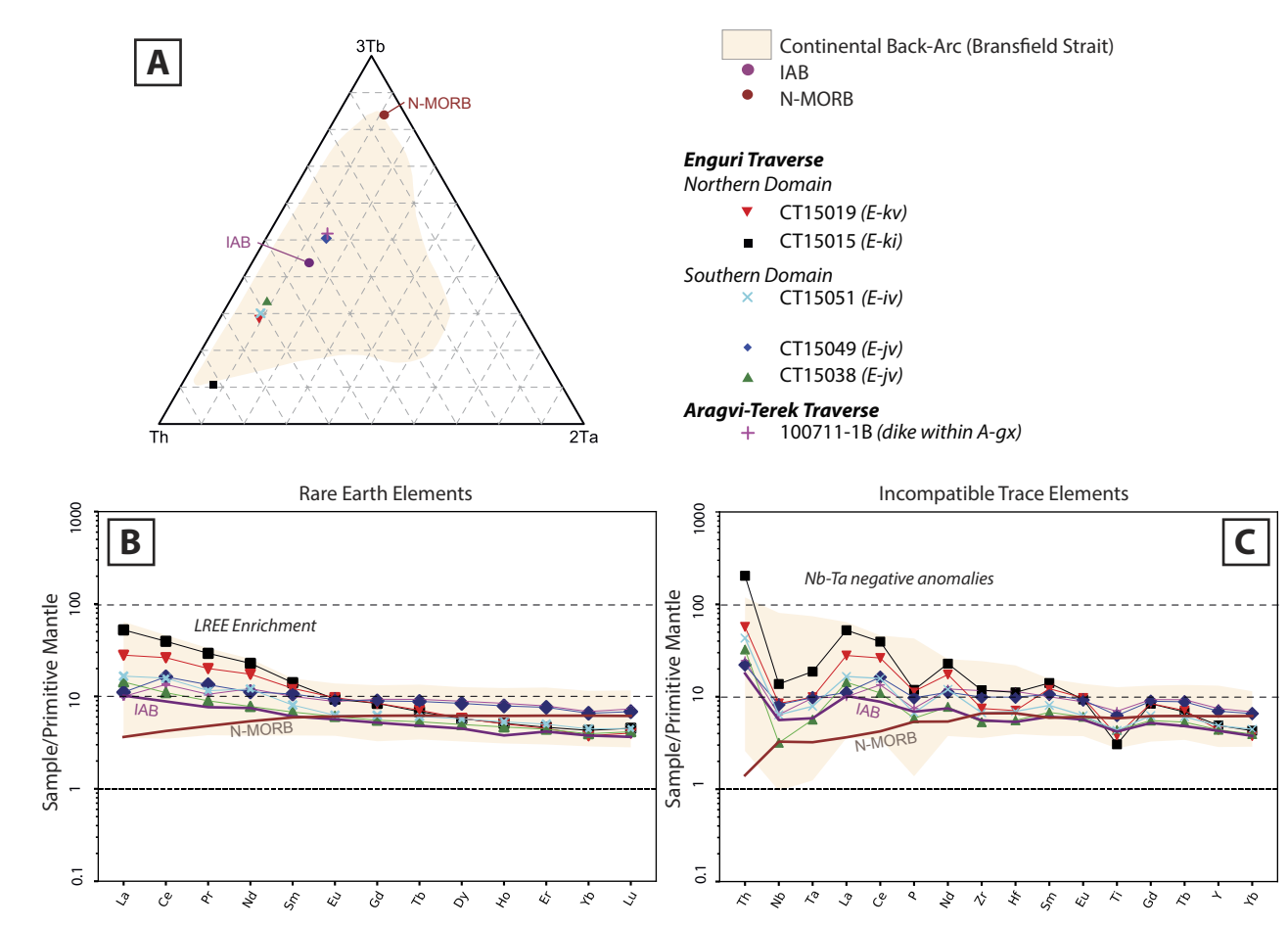


Figure 5. Trace-element geochemical characteristics of Jurassic volcanic/volcaniclastic rocks compared to island-arc basalt (IAB; purple; Kelemen et al., 2003), normal mid-ocean-ridge basalt (N-MORB; brown; Sun and McDonough, 1989), and the continental back-arc basin Bransfield Strait (orange; from Keller et al., 2002; Fretzdorff et al., 2004; Martí et al., 2013), modified from Vasey et al., 2021. Caucasus samples exhibit trace-element characteristics consistent with both island-arc basalt and continental back-arc basin rocks. (A) Th-3Tb-2Ta ternary diagram of Cabanis and Thieblemont (1988), with samples plotting along the Th-3Tb join. (B) Rare earth element (REE) diagram normalized to primitive mantle (McDonough and Sun, 1995), with samples exhibiting light rare earth element (LREE) enrichment. (C) Incompatible trace-element diagram, normalized to primitive mantle (Sun and McDonough, 1989), with samples exhibiting Nb-Ta anomalies.

dominated by a sequence of coarse-grained and massive volcanic breccias that are capped by terrestrial and shallow-marine sedimentary rocks and shelf carbonates. In detail, three units make up the Jvari domain, E-jv, E-js, and E-ils.

Unit E-jv is dominated by massive, coarse, angular volcanic breccia horizons intercalated with generally massive, coarse sandstone intervals. Within the intervening sandstone horizons, rare sedimentary structures (primarily

cross-beds) indicate broadly north-directed paleoflow. Sparse basaltic andesite intrusive dikes crosscut unit E-jv, particularly lower in the stratigraphic section, and in field exposures can be difficult to distinguish from the volcanic breccia. Volcaniclastic rocks within E-jv only contain orthopyroxene, in contrast to units E-kv and E-iv, which contain both orthopyroxene and clinopyroxene. Thin sections of sandstone horizons within E-jv reveal volcanic lithic clasts and extensive carbonate cement. Unit E-jv is the source of a detrital zircon

sample with a maximum depositional age of ca. 157 Ma (reported below in the "Detrital Zircon Analyses of Enquri Rocks" section).

Bedding is poorly expressed within unit E-jv, especially lower in the section. Where observed, bedding strikes are consistent with those in the northern domains, but dips follow the general pattern of shallowing southward, with values of ~50°-70°. Folds in the Jvari domain are typically open, with exposed hinges.

Unit E-js consists of poorly lithified mudstone, shale, and sandstone, as well as massive basaltic andesite volcanic breccia, similar to the volcanic breccia in E-jv (Figs. 4E and 4F). Debris flows are common within the unit, particularly near the stratigraphic base, and decrease in prevalence and thickness up section, from greater than 10 m thick near the base to ~1 m thick near the top. Mudstone and fine sandstone horizons commonly contain organic matter and fragments of petrified wood. Sedimentary structures (primarily cross-bedding) suggest a broadly northward paleoflow direction. Bedding orientations are consistent with those in E-jv, with consistent WNW-strike and moderate (~40°–60°) dips.

Unit E-jls is a fossiliferous, erosionally resistant limestone that forms pronounced flatirons along the range front near Zugdidi (Kandelaki, 1957). In places, unit E-jls exhibits ~1–2-m-thick cyclic bedding, separated by thin shale/marl intervals. East of the traverse, a limestone equivalent to unit E-jls forms a structurally elevated plateau surface between the city of Kutaisi and the town of Tsageri that isolates a syncline cored by Cenozoic strata within the interior of the range (Fig. 1B).

Other Mapped Units

In addition to the units in the tectonostratigraphic domains delineated above, we also mapped several Quaternary units along the Enguri traverse, including debris fans (Qf), landslide deposits (QI), and river terraces (Qt). These units were primarily found south of the range front (e.g., Trexler et al., 2020) and were only mapped when they were greater than 500 m wide or obscured the bedrock geology.

Southern Foreland

Beneath the foreland basin to the south of the main range, seismic data and prior mapping suggest that strata are subhorizontal (Banks et al., 1997; Tibaldi et al., 2017a; Tari et al., 2018). Geomorphic and geologic mapping identified a foreland fold-and-thrust belt ~40 km south of the modern topographic range front (Banks et al., 1997; Tibaldi et al., 2017a), where the core of an anticline exposes Cretaceous limestone (Dzhanelidze and Kandelaki, 1957). Our field observations indicated that this limestone is similar to unit E-jls in outcrop and hand sample, with approximately meter-scale cyclic bedding. The Cretaceous limestone is overlain by a Paleogene–Neogene foreland basin sedimentary section. The fold-and-thrust belt in the Rioni Basin also deforms a flight of river terraces, indicating modern activity (Tibaldi et al., 2017a; Trexler et al., 2020).

Geochemistry of Enguri Volcanic Rocks

We obtained major- and trace-element geochemical analyses on samples collected from volcanic breccia from each of the tectonostratigraphic units that contained a volcanic component: E-kv (Khaishi, sample CT15019), E-iv (Idliani, sample CT15051), and E-iv (Jvari, samples CT15038 and CT15049), together with a dike, E-ki (sample CT15015) that intrudes unit E-ks. We also analyzed a dike intruding crystalline rocks at the northern end of the Terek-Aragvi traverse (sample 100711-1B), which is described below in the "Terek-Aragvi Traverse Tectonostratigraphic Units and Their Bounding Structures" section of the Terek-Aragvi traverse. Results are reported in Table S2 (footnote 1). Samples CT15019, CT15038, and 100711-1B are basaltic in composition, CT15049 is basaltic andesite, CT15051 is basaltic trachyandesite, and CT15015 is trachyandesite. On the Th-3Tb-2Ta ternary diagram (Cabanis and Thieblemont, 1988), all samples plot along the Th-3Tb join, with CT15049 and 100711-1B plotting closest to the 3Tb vertex and CT15015 plotting closest to the Th vertex (Fig. 5A). All samples exhibited light rare earth element (LREE) enrichment, with CT15015 and CT15019 showing the most pronounced enrichment and CT15049 and 100711-1B showing the least pronounced (Fig. 5B). All samples displayed pronounced Nb-Ta negative anomalies (Fig. 5C).

Detrital Zircon Analyses of Enguri Rocks

A previously published detrital zircon analysis from unit E-iv yielded a maximum depositional age of ca. 27 Ma, based on five analyses from the three youngest grains in sample SWGC (Cowgill et al., 2016); this age is considerably younger than the Bajocian (Jurassic) age reported on regional geologic maps (Gamkrelidze and Kakhazdze, 1959). Stratigraphic context gives us reason to question the implied Oligocene maximum depositional age because the sampled unit (E-jv) appears to be stratigraphically down section from fossiliferous Cretaceous carbonate (E-ils). To evaluate this discrepancy, we resampled the same outcrop originally sampled by Cowgill et al. (2016), using field photographs to verify that the two samples were located within ±2 m of one another. Here, we present detrital zircon analyses from this duplicate sample, including an age spectrum and revised maximum depositional age (Fig. 2; Fig. S2). The analyses reported here reproduce the detrital zircon age spectrum of the original SWGC sample, with the exception of the ca. 27 Ma age peak seen in the SWGC sample, despite a larger number of analyses in the replicate sample (128 vs. 106 analyses). We infer that the three Oligocene grains in the original SWGC sample were a contaminant likely introduced during sample processing, and that the maximum depositional age of this unit is ca. 157 Ma, consistent with prior mapping as Bajocian (Middle Jurassic; Fig. 2).

Low-Temperature Thermochronology of Enguri Rocks

We report six new low-temperature thermochronology ages from the Enguri traverse (Fig. 2; Table 1), including three apatite (U-Th-Sm)/He ages

TABLE 1 SUMMARY OF THERMOCHRONOLOGY RESULTS

TABLE 1.30WWATT OF THE TWO OF THE TWO OF THE SOLETO								
Sample	Unit label	Tectonostratigraphic domain	Reported age	Latitude (°N)	Longitude (°E)	Altitude (m)	Apatite (U-Th)/He age [†] (Ma)	Apatite fission- track age [§] (Ma)
Enguri traverse								
AB1027b*	_	Dizi	Silurian-Devonian	43.03902778	42.35536111	870	_	5.49 ± 1.01
AB1028*	E-ds1	Dizi	Mississippian	43.01361111	42.3095	861	_	4.23 ± 0.83
100311-3A	E-ks	Khaishi	Middle Jurassic	42.98740815	42.25974958	733	4.19 ± 0.76	_
CT15047	E-kv	Khaishi	Middle Jurassic	42.95539	42.1937	655	1.93 ± 0.34	_
100411-1	E-iv	Idliani	Middle Jurassic	42.9349221	42.13588784	534	2.68 ± 0.24	_
AB1030*	E-iv	Idliani	Middle Jurassic	42.92311111	42.09055556	567	_	103.95 ± 21.96
AB1018*	-	-	Middle Jurassic	42.4339267	42.743605	274	-	136.55 ± 10.71
Terek-Aragvi	traverse							
CT15092	A-as1	Ananuri	Lower Cretaceous	42.3532	44.70846	1130	6.97 ± 0.06	_
CT15113	A-as1	Ananuri	Lower Cretaceous	42.16097	44.70196	850	5.13 ± 0.81	_

Note: See Supplemental Material (text footnote 1) for full analytical results.

and three previously unpublished apatite fission-track ages from Avdeev (2011). Analytical details are provided in Table S4 (see footnote 1).

We combined these new data with published low-temperature thermochronology from the orogen, using apatite (U-Th-Sm)/He, apatite fission-track, zircon (U-Th)/He, and zircon fission-track systems (Hess et al., 1993; Kral and Gurbanov, 1996; Avdeev, 2011; Avdeev and Niemi, 2011; Vincent et al., 2011, 2020; Vasey et al., 2020). This combined data set provides relatively few vertical transects or analyses of multiple thermochronometric systems on single samples. However, these data provide bounds on the amount of exhumation of the sampled units during the Cenozoic, based on closure temperatures of ~70 °C for apatite (U-Th-Sm)/He (Farley, 2000), ~110 °C for apatite fission track (Gleadow et al., 1983), ~180 °C for zircon (U-Th)/He (Reiners, 2005), and ~230–340 °C for zircon fission track (Tagami, 2005).

Within the Dizi domain, apatite fission-track analyses yielded ages of 5.49 \pm 1.01 Ma (AB1027b) and 4.23 \pm 0.83 Ma (AB1028) (Fig. 2; Table 1). Samples from within the Khaishi domain yielded apatite (U-Th-Sm)/He ages of 4.19 \pm 0.76 Ma (100311–3A) and 1.93 \pm 0.34 Ma (CT15047). All four of these ages are substantially younger than unit depositional ages, which range from Paleozoic (Dizi domain) to Jurassic (Khaishi domain).

The Idliani domain, in the southern half of the Enguri traverse, yielded an apatite (U-Th-Sm)/He age of 2.68 ± 0.24 Ma (100411-1) and an apatite fission-track age of 103.95 ± 21.9 Ma (AB1030). Both ages are younger than the Jurassic depositional age of the samples.

Finally, we report an additional apatite fission-track age from southeast of our mapping traverse, but within units we project along strike to be analogous to the Jvari domain. This sample (AB1018) yielded an age of 136.55 ± 10.71 Ma, younger than the mapped Late Jurassic age of the unit.

■ TEREK-ARAGVI TRAVERSE RESULTS (CENTRAL GREATER CAUCASUS)

Our mapping transect across the central Greater Caucasus followed the Terek and Aragvi Rivers from the Georgia-Russia border near the town of Stepantsminda (42.660°N, 44.641°E) in the north to the town of Jinvali (42.110°N, 44.771°E) ~100 km to the south. The transect spanned from north of the topographic range crest of the Greater Caucasus and across the foreland basin south of the range to within ~40 km of the Georgian capital of Tbilisi (Figs. 1 and 6). While we made field observations south of Jinvali as far as the town of Mtskheta on the outskirts of Tbilisi, we did not map this area at 1:100,000 scale due to lack of exposure. We present each tectonostratigraphic domain and the units within it, in order of exposure from north to south.

Beyond the northern extent of the mapping transect and the Georgia-Russia border, the northern flank of the range at the latitude of the Terek-Aragvi traverse is broken by a north-vergent fold-and-thrust belt (Sobornov, 1994, 1996) that includes active folding in the Terek-Sunzha belt within the northern foreland basin (e.g., Forte et al., 2014). Seismic and well data from the fold-and-thrust belt indicate that it is a thin-skinned feature, similar to the active old-and-thrust belts in the southern foreland Rioni and Kura basins. The fold-and-thrust belt deforms strata that overlie Late Jurassic- to Eocene-age limestone; structures root into a detachment along Jurassic-aged evaporite deposits beneath the carbonate, which in this region is at a depth of ~7 km (Sobornov, 1994, 1996). The northern fold-and-thrust belt accommodates between 30 and 50 km of shortening, and late Miocene-aged strata suggest that deformation in this region did not begin before that time (Sobornov, 1996). South of the fold-and-thrust belt, the strata dip gently northward (~10°-30°)

^{*}Unpublished from Avdeev (2011).

[†]Errors reported at 1 standard error.

[§]Errors reported at 1σ.

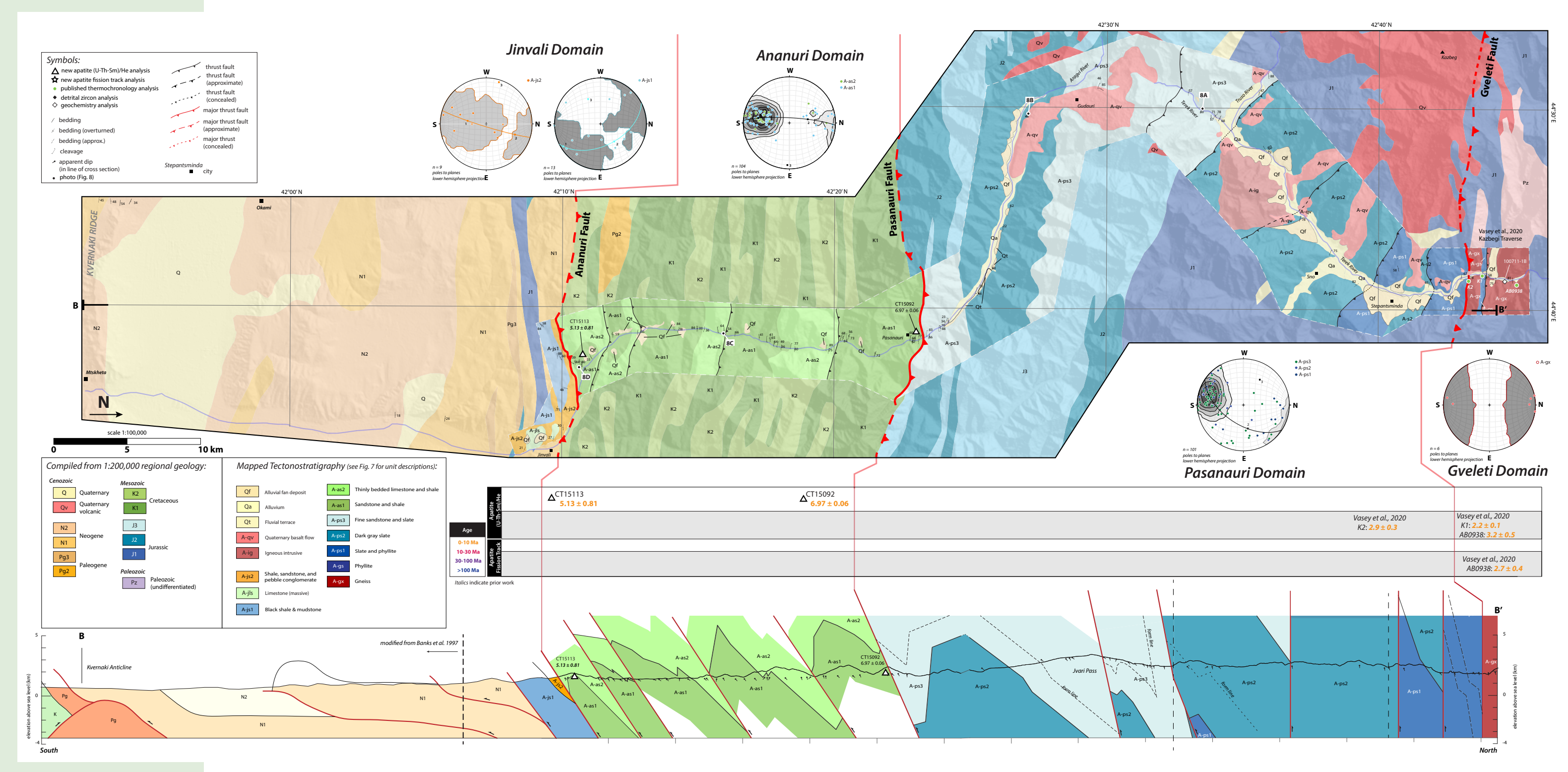


Figure 6. Geologic map of the Terek-Aragvi traverse, central Greater Caucasus (long dimension 108 cm). Bold band in center outlined by white dashed line delineates our 1:100,000 mapping transect. Base map was compiled from 1:200,000 geologic maps (Kandelaki and Kakhazdze, 1957; Gamkrelidze, 1958; Gubkina and Ermakov, 1989). Cross section was compiled from field data and 1:200,000 geologic maps (Kandelaki and Kakhazdze, 1957; Gamkrelidze, 1958; Gubkina and Ermakov, 1989). Stereograms show poles to bedding planes (or, in the case of the Gveleti domain, foliation in gneiss) in an equal-area projection, and they use a Kamb contour with an interval of 5.

along the northern flank of the Greater Caucasus, and several back-thrusts may accommodate additional shortening of >10 km (Sobornov, 1996).

north-northeast-dipping foliation (Vasey et al., 2020). In exposures along the Terek River, this structure, which we call the Gveleti fault, trends roughly NW-SE.

Terek-Aragvi Traverse Tectonostratigraphic Units and Their Bounding Structures

Along the Terek-Aragvi traverse (A), we identified four distinct tectonostratigraphic domains: Gveleti (g), Pasanauri (p), Ananuri (a), and Jinvali (j), which are composed of three rock types, crystalline rocks (x), clastic sedimentary rocks dominated by interlayered sand and mudstone (s), and limestone (ls), with a total of 10 discrete map units (Figs. 6 and 7). The Gveleti domain consists of a crystalline unit (A-gx) and a metasedimentary unit (A-gs). The Pasanauri domain contains three distinct clastic units (A-ps1, A-ps2, and A-ps3). The Ananuri domain contains two distinct clastic units (A-as1 and A-as2). The Jinvali domain is a mixed clastic and carbonate domain (A-js1, A-js2, and A-jls). The eastern traverse notably lacks volcaniclastic sequences similar to those along the Enguri traverse to the west (E-iv, E-kv, and E-jv). Bedding strike was observed to be remarkably consistent along the Terek-Aragvi traverse and varied only ±~20° from the average (stereograms, Fig. 6), similar to the Enguri traverse, with average strike direction rotating ~20° clockwise, from ~270°–280° in the north to ~290°–300° in the south.

Gveleti Domain: Granodiorite and Metasedimentary Rock

Unit A-gx is granodiorite of the Dariali Massif, exposed along the Terek River north of Stepantsminda (Gubkina and Ermakov, 1989). This unit is locally gneissic and intruded by numerous subvertical mafic dikes that are subparallel to one another and to compositional banding in the granodiorite. Intrusive dikes contain pyroxene and feldspar phenocrysts in a medium-coarse basaltic groundmass.

Unit A-gs is a metasedimentary unit that is dominated by dark-gray slate and phyllite in outcrops along the Terek River and is flanked by A-gx to both the south and north. Contact relationships between units A-gx and A-gs are enigmatic and could be depositional or structural, although an intrusive relationship is precluded by the older age of A-gx relative to A-gs (Vasey et al., 2020). Prevalent secondary mineralization includes quartz veins and equant pyrite (up to centimeter scale). Bedding is subvertical to steeply north dipping (80°). Well-developed cleavage is generally more prominent and more steeply dipping than bedding, and the two can be difficult to distinguish.

Gveleti Fault

The southern margin of A-gx is defined by a shear zone that juxtaposes the granodiorite to the north against fine-grained metasedimentary rocks of the Pasanauri domain to the south. The shear zone itself is characterized by mylonitization of granodiorite, hydrothermal alteration and quartz veins, and dominantly steeply

Pasanauri Domain: Phyllite, Slate, and Marl

Unit A-ps1 consists of dark-gray slate and phyllite. Secondary mineralization in the form of quartz veins and equant pyrite (up to centimeter scale) is found in many outcrops. Bedding is steeply north dipping (~80°) to subvertical, with consistent WNW strike. Well-developed cleavage is typically more prominent than bedding.

Unit A-ps2 is composed primarily of dark-gray slate. The contact between A-ps1 and A-ps2 is not directly exposed, but structural orientations across it are consistent, and so we infer it to be depositional and conformable. Within exposures of A-ps2, 30–50-cm-thick tabular and laterally continuous sandstone beds punctuate otherwise slaty outcrops; some contain horizons of normally graded bedding ~10 cm thick. Well-developed cleavage is typically present and is as well expressed in outcrop as is bedding. Bedding within A-ps2 remains steeply north dipping (~80°) to subvertical, with consistent WNW strike. Folds within A-ps2 are commonly visible in hillsides and typically have hinge zones ~100 m wide.

Unit A-ps3 is characterized by ~1–3-m-scale beds of sandstone, muddy limestone, and marl, punctuated by thin (~10 cm) horizons of slate. In outcrop, well-developed scours and load casts are commonly present on coarse-grained bed bases. The abundance and thickness of slate/shale horizons vary geographically, with marl and sandstone more abundant north of Gudauri (Fig. 8) and slate and mudstone dominant to the south. Bedding within A-ps3 remains WNW-striking and primarily north dipping (50°-80°; Fig. 6). Unit A-ps3 breaks with a conchoidal fracture pattern, and fine-grained horizons are slaty but not phyllitic.

Pasanauri Fault

The inferred Pasanauri fault juxtaposes unit A-ps3 to the north against unit A-as1 to the south. The contact is inferred to be structural based on abrupt changes in induration, rock type, layering, and structural style. South of the Pasanauri fault, the Ananuri domain is characterized by unmetamorphosed sedimentary rocks with poor cleavage. Rock types include sandstone, shale, marl, and limestone, the latter of which is uncommon within A-ps3. Sedimentary structures are common within the Ananuri domain, in contrast to units north of the Pasanauri fault (other than A-ps3), where they are difficult to identify. Bedding in the Ananuri domain is quite rhythmic, with beds rarely thicker than 1 or 2 m. The Ananuri domain is deformed by regularly spaced faults and localized zones of disharmonic folding.

Ananuri Domain: Interbedded Marine Sandstone, Marl, and Limestone

Unit A-as1 is characterized by interbedded sandstone and dark-gray to black shale. Beds are generally 0.5–2 m thick, and grading and cross-bedding

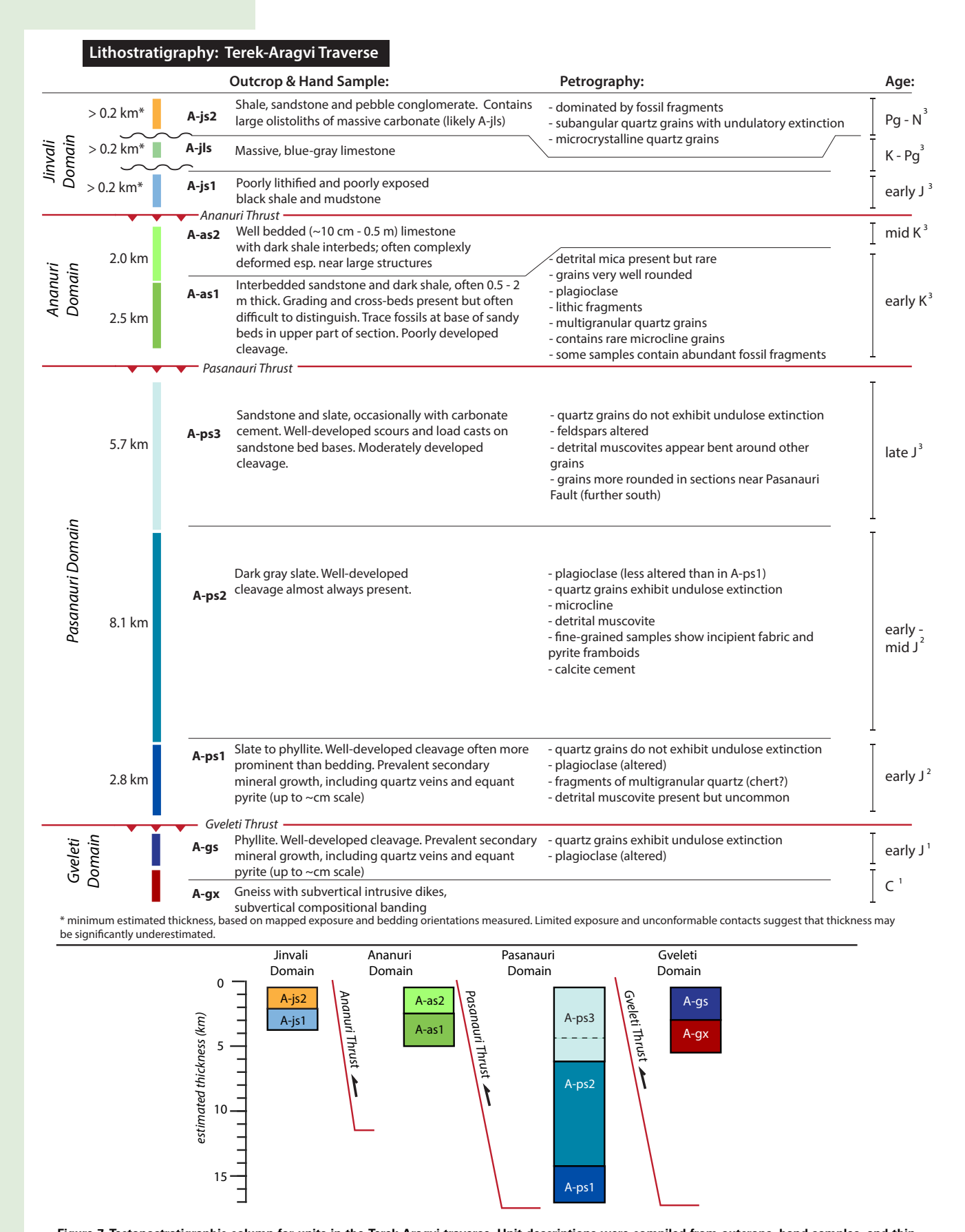


Figure 7. Tectonostratigraphic column for units in the Terek-Aragvi traverse. Unit descriptions were compiled from outcrops, hand samples, and thin sections. Unit thicknesses were estimated based on mapping and structural data. References for mapped age: 1—Vasey et al. (2020); 2—Gubkina and Ermakov (1989); 3—Kandelaki and Kakhazdze (1957). N—Neogene; Pg—Paleogene; K—Cretaceous; J—Jurassic; C—Carboniferous; DZ—detrital zircon.

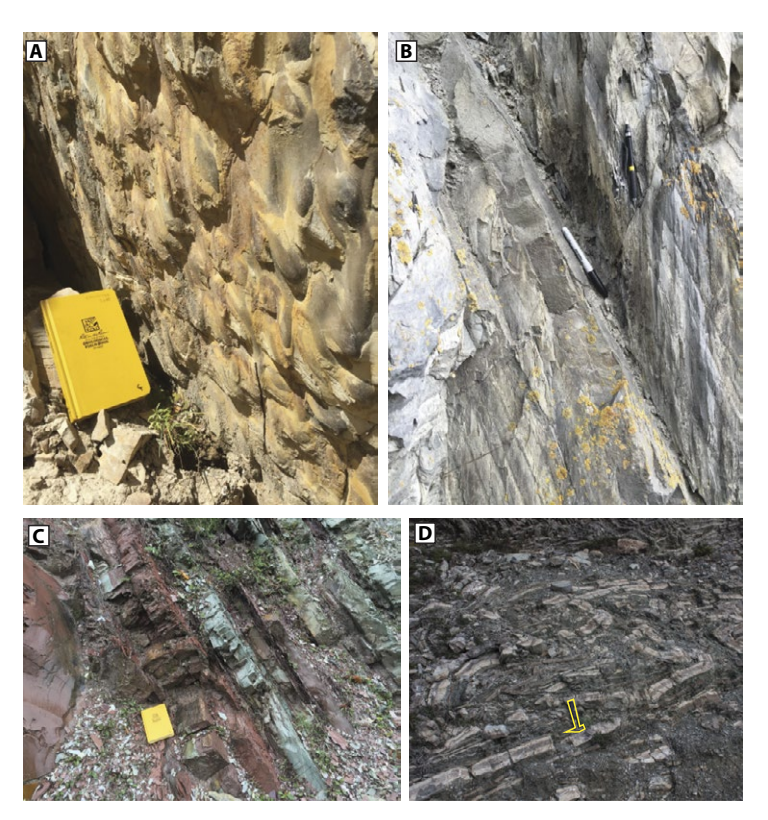


Figure 8. Field photographs. (A) Scour casts at the base of a coarse bed within A-ps3. Field of view is ~2 m wide. Facing NW. (B) A-ps2 shows strongly developed cleavage (in orientation of black and yellow pencil), which is nearly as prominent as bedding (in orientation of gray and black marker) in some outcrops. Facing SE. (C) At the southern end of the Terek-Aragvi traverse, limestone and marl of unit A-as2 have rhythmic, ~1-m-thick bedding. Facing W. (D) Near the top of unit A-as2, deformation is highly disharmonic near fold hinges and faults (hammer for scale). Facing W.

are regularly present. Trace fossils are abundant at the bases of sandy beds in the upper part of the section. Paleoflow direction is southward, based on sedimentary structures. Poorly developed axial planar cleavage, more steeply dipping than bedding, is present in outcrops of A-as1 and is less distinct than bedding.

A gradational contact separates units A-as1 and A-as2 and is defined by the first appearance of prominent limestone horizons in outcrop. Unit A-as2 is distinguished by rhythmic, thinly bedded (~0.1–0.5 m) limestone with dark shale interbeds. Internal to this unit, there is a distinctive package of red shale, green marl, and limestone that is ~10 m thick and stratigraphically bounded both above and below by gray shale and limestone. While bedding orientations

are generally consistent with map-scale structures, this unit locally exhibits complex and disharmonic deformation near large structures.

Bedding dips within the Ananuri domain are ~40–60°N, in contrast to the typically subvertical dips within the Pasanauri domain. Anticlines typically have southern limbs that are steeply south dipping to overturned. Within this domain, fold hinge zones are typically only a few meters wide. We also documented an increase in disharmonic deformation and flexural slip at fold hinges, particularly evident in A-as2 (Fig. 8).

Ananuri Fault

The Ananuri fault is the structural boundary between the Ananuri domain to the north and the less well-exposed Jinvali domain to the south. The fault dip is ~45°N, constrained by the maximum dip of bedding in its hanging wall.

Jinvali Domain: Olistostrome, Mixed Sandstone and Conglomerates, and Massive Carbonate

The Jinvali domain, in the footwall of the Ananuri fault, is lithologically distinct from the Ananuri, Pasanauri, and Gveleti domains to the north. While the units farther north are consistently fine-grained siliciclastic and carbonate deposits, the Jinvali domain contains a variety of sedimentary rocks, including coarse sandstone, pebble conglomerate, and massive limestone, in addition to fine mudstone and shale.

Unit A-js1 is characterized by poorly lithified black shale and mudrock that are generally poorly exposed. The stratigraphic bottom of unit A-js1 was not observed along our mapping traverse. Channelized interbeds of medium- to fine-grained sandstone, 1–3 cm thick, punctuate outcrops of A-js1. Cross-bedding and trace fossils within sandstone lenses provide stratigraphic facing direction. Sedimentary structures indicate variable paleoflow directions that are broadly north directed.

Unit A-jls is a massive, coarse-grained, and blocky gray limestone, with exposure limited to the southeastern corner of the mapping transect. The contact relationship between units A-js1 and A-jls was unclear due to poor exposure. In the vicinity of the Jinvali Dam, A-jls is unconformably overlain by unit A-js2. Outcrops of unit A-jls are not laterally continuous, and bedding orientation and continuity were difficult to determine.

Unit A-*j*s2 unconformably overlies units A-*j*s1 and A-*j*ls and consists of interbedded shale, sandstone, and coarse sand to pebble conglomerate. Sandstone and conglomerate lenses are variable in thickness, discontinuous at outcrop scale, matrix supported, and composed of well-rounded quartz grains and lithic fragments. This unit contains blocks of coarse clastic rock, as well as large (up to ~10 m diameter) blocks of massive carbonate that appear to have been sourced from unit A-*j*ls, enveloped by finer-grained deposits.

Other Mapped Units

A-ig is an igneous intrusive unit exposed in the northern half of the Terek-Aragvi traverse, reported as Cenozoic in age (Gubkina and Ermakov, 1989). This unit is most identifiable by the dramatic topography it supports, most notably in a peak along the east side of the road ~10 km south of Stepantsminda (Fig. 6). Outcrops in the river valleys or near the road define prominent edifices that are flanked by large debris fans. Map patterns suggest that this unit intrudes, and postdates, units A-ps1 and A-ps2 (Fig. 6).

Quaternary basaltic extrusive volcanic flows (A-qv) are also common in the northern half of the Terek-Aragvi traverse. These flows are commonly clearly expressed topographically, filling drainages and abutting valley walls. Based on map patterns, many of these flows appear to have been sourced from Mount Kazbeg, although other vents may also be present.

We also mapped Quaternary cover units when they obscured the bedrock geology along the traverse. We identified these as abandoned river terraces (Qt), alluvial deposits (Qa), or debris fans (Qf).

Southern Foreland (Okami and Kvernaki Anticline)

A fold-and-thrust belt deforms the foreland basin up to several tens of kilometers south of the topographic range front and is bounded to the south by north-directed structures associated with the Achara-Trialet thrust belt in the Lesser Caucasus region south of the transect (see "Geologic Setting" section; Banks et al., 1997; Alania et al., 2017). While it is likely that some of these structures are active and linked to the Greater Caucasus, the structural complexity of the region obscures linkages between the fold-and-thrust belt and structures in either the Greater Caucasus or the Achara-Trialet thrust belt (Banks et al., 1997; Szymanski, 2005).

Low-Temperature Thermochronology of Terek-Aragvi Rocks

We report two new low-temperature thermochronology ages from the central Terek-Aragvi traverse (Fig. 6; Table 1). In the northern part of the Ananuri domain, in the central part of the traverse, sample CT15092 yielded an apatite (U-Th-Sm)/He age of 6.97 ± 0.06 Ma. At the southern end of the Ananuri domain, sample CT15113 yielded an apatite (U-Th-Sm)/He age of 5.13 ± 0.81 Ma. Both ages are considerably younger than the Cretaceous depositional ages of the units sampled.

DISCUSSION OF THE ENGURI TRAVERSE

The style and expression of deformation change distinctly from north to south along the Enguri traverse. In the northern Dizi and Khaishi domains, folds are typically isoclinal, and of large enough scale that they often are not observable within a single outcrop; in the southern Idliani and Jvari domains, folds exhibit asymmetric limb dips, generally with anticlines verging to the south, and hinge zones that are localized enough so as to be observed at the outcrop scale. Changes in metamorphic grade commonly occur across faults, particularly at the northern end of the mapping traverse, and they were used to help identify locations of otherwise poorly exposed structures (see "Geochemistry of Enguri Volcanic Rocks" section). We interpret these increases in bedding dip, extent of deformation, and metamorphic grade along the mapping traverse to represent a northward increase in exhumation depth, such that the thrust sheets at the northern end of the traverse represent a deeper stratigraphic and/or structural level than those of lower metamorphic grade farther south.

Evidence for Major Structures

Our data from the Enguri traverse suggest that the western Greater Caucasus is subdivided by at least three or four major faults, each with the potential for a significant amount of displacement (tens of kilometers). In each case, the fault location and orientation we mapped are consistent with mapped lithologic boundaries on 1:100,000 and 1:200,000 scale geologic maps (e.g., Gamkrelidze and Kakhazdze, 1959; Dzhanelidze and Kandelaki, 1957; Zdilashavili, 1957; Kandelaki, 1957; Gubkina and Ermakov, 1989; Gamkrelidze, 1958; see also section on "Definition of Georgian Tectonostratigraphy"). In our field experience with these maps, faults are inconsistently identified, and age determinations are not always reliable, but lithologic boundaries are generally well located. As a result, we feel confident in using the lithologic boundaries on published maps to extrapolate faults across mapping transects and along strike. Where possible, we inferred fault dip based upon constraints from map patterns of fault traces (i.e., changes in contact orientation across topography).

The broad correlation between bedding strike and orientation of major faults is consistent with the interpretation of the Greater Caucasus having undergone one major tectonic episode since Mesozoic time (namely, the closure and inversion of the Greater Caucasus Basin; see "Background" section). Our structural data, which show remarkably consistent bedding orientations both along and across strike, indicate only one tectonic episode. In this context, the dip of bedding provides a minimum bound on fault dip, assuming that faults formed in previously undeformed stratigraphy and must cut up section or parallel to bedding.

Several structures we identified, e.g., the Ushba and Dizi faults, have been previously described (Dotduyev, 1986; Adamia et al., 2011b; e.g., Somin, 2011; Vasey et al., 2020) and clearly accommodate significant (i.e., multiple kilometers) displacement based on the different rock types and metamorphic grades they juxtapose. We argue that the Idliani and Khaishi faults likely also accommodate significant displacement and play a major role in the structural architecture of the orogen, based on evidence from (1) sediment provenance and basin paleogeography, (2) volcanic provenance, and (3) low-temperature thermochronology. This suite of four major faults acts as an imbricate fan to

accommodate shortening within the orogen, and we interpret steeper dips of bedding on the northern portion of the traverse to be a result of in-sequence stacking of new thrust sheets beneath the growing imbricate fan.

Evidence from Sediment Provenance and Basin Paleogeography

Sedimentary rocks from the northern and southern ends of the traverse exhibit discrete provenance signatures, suggesting that one or more structures within the traverse may represent a major tectonic boundary. Sedimentary rocks from the Dizi and Khaishi tectonostratigraphic domains can be grouped into a single suite with similar provenance, based on distinctive grains and clasts, paleoflow directions, and sedimentary facies. Within the Dizi and Khaishi domains at the northern end of the Enguri traverse, units E-ds2, E-ks, and E-iv contain quartz grains showing evidence of strain (undulose extinction of grains in thin section), but otherwise they do not show evidence of metamorphism beyond cleavage development. While EBSD analysis of a sample within this unit did show minor alignment of crystallographic axes (see Supplemental Text and Fig. S3), this is inconsistent with the kinematics represented by the macroscopic fabric and likely indicates an inherited fabric. The lack of metamorphic phases and fabric development in the unit itself, combined with the existence of a weak, inherited crystallographic fabric, leads us to conclude that the metamorphism of the unit itself was relatively low, and that strained quartz grains in unit E-ds2 are detrital and indicate a metamorphic unit contributed as a sediment source rather than indicating strain of the sample after deposition. Because the grains are detrital within the most metamorphosed unit (E-ds2) of the domain, we interpret the strained quartz grains in the less-metamorphosed to unmetamorphosed samples (e.g., units E-ds1, A-ps2, A-js2) to be detrital as well. Samples from the northern (Dizi and Khaishi) tectonostratigraphic domains also contain detrital strained quartz and mica grains and are fine grained and apparently distal from the sediment source. The presence of metamorphic grains and the southward paleoflow directions indicated by sedimentary structures together suggest that these sediments were sourced from the north.

In contrast, the Jvari domain, at the south end of the Enguri traverse, conspicuously lacks the detrital mica and strained quartz that characterize the tectonostratigraphic domains north of the Idliani and Khaishi faults. Instead, the Jvari domain contains abundant volcanic and volcaniclastic lithic fragments and exhibits secondary calcite. Sedimentary units within the Jvari domain also appear to have been deposited in a proximal setting, as indicated by coarse sandstone, gravel, and petrified wood, none of which is seen in the sedimentary units farther north. Sedimentary structures within the Jvari domain indicate northward paleoflow.

This suggests that units within the Jvari domain did not receive sediment from the same source areas as units in the northern (e.g., Khaishi) domains. These observations are consistent with detrital zircon analyses, in which samples from areas south of the Idliani fault show almost exclusively 180–160 Ma ages (Fig. 2; Fig. S2), while samples from further north along the traverse

(e.g., WGC-1, 2 from Tye et al., 2021; N2, N3 from Vasey et al., 2020) have both mid-Jurassic and Paleozoic peaks. Whether unit E-iv within the Idliani domain itself belongs to the northern or southern sedimentary package is difficult to discern based on field observations, in part due to the poor exposure of this unit.

Published maps (Gamkrelidze and Kakhazdze, 1959) indicate that much of the sedimentary section along the Enguri traverse was deposited during Middle to Late Jurassic time. If these age assignments are correct, then the discrete northern and southern sedimentary provenance regions appear to have been fed into the Greater Caucasus marine basin more or less simultaneously (e.g., Cowgill et al., 2016, 2018). However, because independent confirmation of these ages is lacking, it is also possible that the differences between the northern and southern domains represent a temporal shift in provenance, with one of the provenance regions being older than the other.

Evidence from Multiple Discrete Volcanic Sources

We interpret, based on field and laboratory observations, that the volcanic and volcaniclastic units from the Khaishi, Idliani, and Jvari domains are derived from at least two discrete volcanic sources, separated geographically by the Idliani fault. We separated these units into a northern group (units E-kv and E-iv) and a southern group (unit E-iv), as described below.

Outcrops of the northern group, in particular, unit E-kv, are characterized by distinct horizons of coarse breccia and pillow lava interspersed within finer-grained sedimentary intervals. In contrast, unit E-jv of the southern group is defined by continuous exposure of massive volcanic breccia with few marker beds or other indicators of stratigraphic layering and facing direction.

Major- and trace-element geochemistry analyses support the distinction that we drew from field and thin-section observations. In particular, sample CT15019 from unit E-kv exhibited stronger LREE enrichment than samples CT15038 and CT15049 from unit E-jv (Fig. 5B), consistent with (though not uniquely indicative of) separate volcanic sources. Sample CT15015 in unit E-ki also exhibited strong LREE enrichment (Fig. 5B); however, this sample contained ~60 wt% SiO₂, and this pattern may be the result of fractional crystallization of a more primitive melt. Additional geochemical analyses are needed to determine if these contrasting REE patterns are consistent across the Khaishi fault.

Evidence from Low-Temperature Thermochronology

The compiled low-temperature thermochronology results we report from the Enguri traverse are not numerous enough for detailed thermal modeling, but they do provide important constraints on exhumation magnitude and timing across structures along the traverse. In order to discuss these constraints, we classified samples as either "collisional" or "precollisional," as a shorthand for whether the sample in question was exhumed during growth of the modern Greater Caucasus (collisional, thermochronometric ages younger

than ca. 30 Ma) as opposed to being either detrital or exhumed prior to the Cenozoic onset of Arabia-Eurasia collision (precollisional, thermochronometric ages older than ca. 35 Ma; Avdeev and Niemi, 2011; Vincent et al., 2011, 2007).

Samples that we refer to as "collisional" have been buried deeply enough to exceed closure temperature of the thermochronometric system in question and then exhumed, thus exhibiting thermochronometric ages that are younger than both the depositional or crystallization age of the rock analyzed and the presumed timing of onset of the Arabia-Eurasia collision at 30 Ma. For sedimentary and extrusive volcanic rocks, thermochronometric ages younger than 30 Ma must reflect a history of postdepositional burial and subsequent exhumation. For intrusive igneous or metamorphic rocks, these ages may reflect postcrystallization/metamorphic cooling, reburial and exhumation, or primary exhumation (for more details, see Supplemental Material [footnote 1]).

For apatite (U-Th-Sm)/He analyses, the boundary between collisional and precollisional samples is located between the Idliani domain (collisional sample 100411–1) and the Jvari domain (precollisional sample WG28c/5 in the Chanis River section; Fig. 2; Vincent et al., 2011). Along the Tskhenis River, ~60 km east of the Enguri transect, we interpret published analyses (Vincent et al., 2011) to indicate that this boundary is between presumed collisional sample WG137/1, which is along strike of the Dizi domain, and precollisional samples W66c/2 and WG67/8, which are along strike of the Jvari domain (Figs. 1and 2; Fig. S4A). We presume sample WG137/1 is collisional in the apatite (U-Th-Sm)/He system based on its collisional apatite fission-track age and the higher closure temperature of the apatite fission-track system relative to the (U-Th-Sm)/He system.

In the apatite fission-track system, the boundary between collisional and precollisional ages is located farther to the north in the orogen than in the apatite (U-Th-Sm)/He system, between the Dizi domain (collisional fission-track sample AB1028) and the Idliani domain (precollisional sample AB1030; Fig. 2). Because the apatite fission-track system records a higher closure temperature than the apatite (U-Th-Sm)/He system, this indicates a gradient of increasing exhumation levels from south to north along the traverse.

In the zircon (U-Th)/He system, we infer that the boundary between collisional and precollisional ages lies south of the Ushba domain, based upon collisional ages of samples N3 and N1 (Vasey et al., 2020), which straddle the Ushba thrust, and samples A1, T3, and T1 (Avdeev, 2011; Avdeev and Niemi, 2011) in the crystalline basement of the Ushba domain (Figs. 1 and 2). Although precollisional ages have yet to be reported from the southern part of the Enguri traverse, we infer that the boundary in this system is no farther south than the Idliani domain (precollisional apatite fission-track sample AB1030, with a lower closure temperature relative to the zircon [U-Th]/He system; Fig. 2). No reset zircon fission-track or ⁴⁰Ar/³³Ar ages have been reported from the Caucasus (e.g., Avdeev and Niemi, 2011); thus, maximum Cenozoic exposure levels for much of the Greater Caucasus appear to be no greater than depths equivalent to paleotemperatures of ~<220 °C.

Apatite (U-Th-Sm)/He analyses reported by Vincent et al. (2011) from the Chanis and Tskhenis River sections were performed on aliquots consisting of 2–4 grains each, with ages reported as the mean of three to four replicate

analyses for each sample. Because the reported ages are all older than (Tskhenis), or equal to (Chanis), the reported depositional ages, it appears that these are analyses of detrital grains, the ages of which were either unreset or only partially reset after deposition. In such a case, each individual apatite grain is expected to have a different (U-Th-Sm)/He age. Thus, the meaning of the mean ages as reported in the original publication is not clear because multiple grains (2–4) of potentially variable age were analyzed in each of the three to four replicate analyses that were then averaged. However, because the samples appear to have detrital or only partially reset (U-Th-Sm)/He ages, we conclude that the break in apatite (U-Th-Sm)/He ages occurs north of these samples.

Structural Geometry of the Enguri Traverse

Based on our stratigraphic, structural, and thermochronologic data, we infer that the Enguri traverse is subdivided by at least four major structures—the Ushba, Dizi, Khaishi, and Idliani faults. Each fault separates two distinct tectonostratigraphic packages, with differing metamorphic grade (e.g., the Dizi fault, separating the Dizi and Khaishi domains), sedimentary provenance (e.g., the Idliani fault, separating the Idliani and Jvari domains), deformation style (e.g., the Ushba fault, separating the crystalline core from the Dizi domain), and/or thermal histories (e.g., the Idliani fault in the apatite [U-Th-Sm]/He system and the Khaishi fault in the apatite fission-track system). Given these differences, particularly with sedimentary provenance and metamorphic grade, each of these faults may accommodate significant magnitudes of shortening (i.e., potentially tens of kilometers or more). Together, the Ushba, Dizi, Khaishi, and Idliani faults divide the mapping traverse into a broadly south-vergent imbricate stack (e.g., Fig. 2).

Limited exposure along the traverse restricts more detailed investigation of the structures themselves. Detailed offset estimates across these tectonostratigraphic domain–bounding faults identified here cannot be quantified due to the lack of stratigraphic correlation across them or field exposures of hanging-wall cutoffs. Similarly, lack of direct exposure of the structures themselves requires that fault geometry be inferred based on the surrounding geometries. Faults in the northern half of the traverse have inferred dips of >~70°N, constrained by the orientation of bedding in the hanging wall. In these cases, we assume that these structures initially formed in-sequence and cut upward through bedding, an inference supported by structural data (Fig. 2), though these data do not preclude other interpretations.

■ DISCUSSION OF THE TEREK-ARAGVI TRAVERSE

Evidence for Major Structures along the Terek-Aragvi Traverse

Our data from the Terek-Aragvi traverse suggest that several major faults subdivide the central Greater Caucasus into tectonostratigraphic domains,

much like the Enguri traverse, with each fault potentially accommodating significant (tens of kilometers) displacement. In cases where we did not directly observe fault planes, we inferred fault orientations that are consistent with observed exposures. Using the same constraints as we did along the Enguri traverse (see "Evidence for Major Structures" section), we constrained fault location and orientation using our own mapping and mapped lithologic boundaries on 1:100,000 and 1:200,000 scale regional geologic maps (e.g., Gamkrelidze and Kakhazdze, 1959; Dzhanelidze and Kandelaki, 1957; Zdilashavili, 1957; Kandelaki, 1957; Gubkina and Ermakov, 1989; Gamkrelidze, 1958; see "Definition of Georgian Tectonostratigraphy" section). Where possible, we inferred fault dip based upon constraints from map patterns of fault traces (i.e., changes in contact orientation across topography). Similarly, we inferred that the dip of bedding provides a maximum bound on fault dip, assuming that faults formed in previously undeformed stratigraphy and must cut up section or parallel to bedding.

Along the Terek-Aragvi traverse, the Gveleti and Ananuri faults (at the northern end and southern end of the traverse, respectively) appear to be major structures, based on changes in both rock type and either metamorphic grade (Gveleti) or sedimentary provenance (Ananuri). The intervening portion of the Terek-Aragvi traverse does not seem to contain any fundamental breaks in depositional setting or sediment provenance.

The Gveleti fault appears to be a major structure based upon the juxtaposition of tectonostratigraphic units (granodiorite to the north, and fine-grained metasedimentary rocks to the south) and the presence of a mylonitic shear zone (Vasey et al., 2020). In keeping with prior work referring to this structure as the Main Caucasus thrust (Mosar et al., 2010), this structure may be analogous to the Ushba fault along the Enguri traverse to the west, where Paleozoic crystalline basement is emplaced over metasedimentary rocks. Due to the lithologic complexity of the Gveleti domain, the Gveleti fault is not as clearly expressed as the Ushba fault.

We concluded that the Ananuri fault is a major structure from the differences in rock type and sediment provenance between the Ananuri and Pasanauri domains to the north and the Jinvali domain to the south. Specifically, the Ananuri and Pasanauri domains are dominated by marl and shale, whereas the Jinvali domain contains approximately meter-scale limestone olistolith, massive carbonate, pebble conglomerate, and coarse sandstone. In thin section, rocks north of the Ananuri fault contain detrital mica and lack volcanic lithic grains, whereas those to the south lack detrital mica and contain volcanic lithic clasts not seen elsewhere on the traverse. Prior studies have similarly reported limestone olistoliths enveloped in a muddy to sandy matrix within the Jinvali domain, with the blocks being inferred to have been derived from the southern flank of the Greater Caucasus marine basin (Banks et al., 1997; Cowgill et al., 2016). The significant differences between the tectonostratigraphic domains to the north and south of the Ananuri fault suggest this structure accommodated approximately tens of kilometers or more displacement, resulting in the juxtaposition of different portions of the original sedimentary basin.

Metamorphism is phyllite grade or lower along the entire traverse and decreases from north to south, which we interpret to represent a southward decrease in exhumation depth. The only prior thermochronology results reported along the Terek-Aragvi traverse are those from Vasey et al. (2020), which are confined to the northern end of the traverse and thus limit the conclusions we can draw. However, the two apatite (U-Th-Sm)/He ages reported here are both collisional (younger than 30 Ma), indicating that the boundary between collisional and precollisional apatite (U-Th-Sm)/He ages is well south of the Pasanauri fault, potentially as far south as the Ananuri fault, nearly at the southern end of the mapping traverse (Fig. 6), or beyond. Because apatite fission-track and zircon (U-Th)/He ages for sample AB0938 within the Gveleti domain are also collisional (Vasey et al., 2020), the boundaries between collisional and precollisional samples in these two systems are inferred to lie south of this domain, although this provides little constraint considering that this sample is near the north end of the traverse.

Structural Geometry of the Terek-Aragvi Traverse

The Gveleti, Ananuri, and Pasanauri faults divide the Terek-Aragvi traverse into a south-directed imbricate thrust stack in which bedding dips increase northward. At the northernmost end of the mapping traverse, subvertical fault dips are inferred based on the maximum dip of bedding in the footwall and an assumption that faults cut either parallel to bedding or up section. In the latter case, the faults may in fact be overturned and dip steeply south. We found no evidence of major back-thrusts or out-of-sequence thrusting along this traverse.

The Terek-Aragvi traverse consists of marine basin sedimentary deposits along its entire length, with the lack of Mesozoic volcanic or volcaniclastic deposits here standing in marked contrast to the Enguri traverse to the west. Because the two traverses are separated by over 100 km along strike, we suggest that this difference in rock type results from along-strike variation in the depositional setting, source areas, and overall geometry of the depocenter(s) in which these units were deposited within the Greater Caucasus Basin. More work is needed, particularly in the region between the two traverses we present here, to further explore the reasons for these differences.

■ IMPLICATIONS FOR OROGEN-SCALE STRUCTURE AND THE CONTINUITY OF MAJOR STRUCTURES ALONG STRIKE

Integration of our lithologic and structural observations with published 1:200,000 scale geologic maps (Dzhanelidze and Kandelaki, 1957; Kandelaki, 1957; Zdilashavili, 1957; Gamkrelidze, 1958; Gamkrelidze and Kakhazdze, 1959; Gubkina and Ermakov, 1989) leads us to suggest that the major thrust faults identified on each traverse are continuous along strike of the range and can be extrapolated from one traverse to the next by correlating the lithologic and structural boundaries observed along the traverses. Published thermochronologic

observations in the western Greater Caucasus (Hess et al., 1993; Kral and Gurbanov, 1996; Avdeev, 2011; Avdeev and Niemi, 2011; Vincent et al., 2011, 2020; Vasey et al., 2020) provide support for these along-strike correlations (Fig. 9). We collectively refer to these structures as the North Georgia fault system (Fig. 10).

Faults within the North Georgia fault system are often steeply (>60°) dipping, particularly in the core of the range. However, in most cases, these faults are shallowly dipping relative to the bedding in the hanging wall, suggesting they formed as low-angle faults. Based upon this geometric relationship, we suggest that the North Georgia fault system represents a series of originally low-angle thrusts, each with multiple kilometers of horizontal displacement, rather than a series of high-angle, reactivated reverse faults with primarily vertical displacement.

North Georgia Fault System: Correlating Major Structures Along Strike

Prior work has proposed multiple structures that extend along strike of the Greater Caucasus (e.g., Philip et al., 1989; Allen et al., 2004; Mosar et al., 2010;

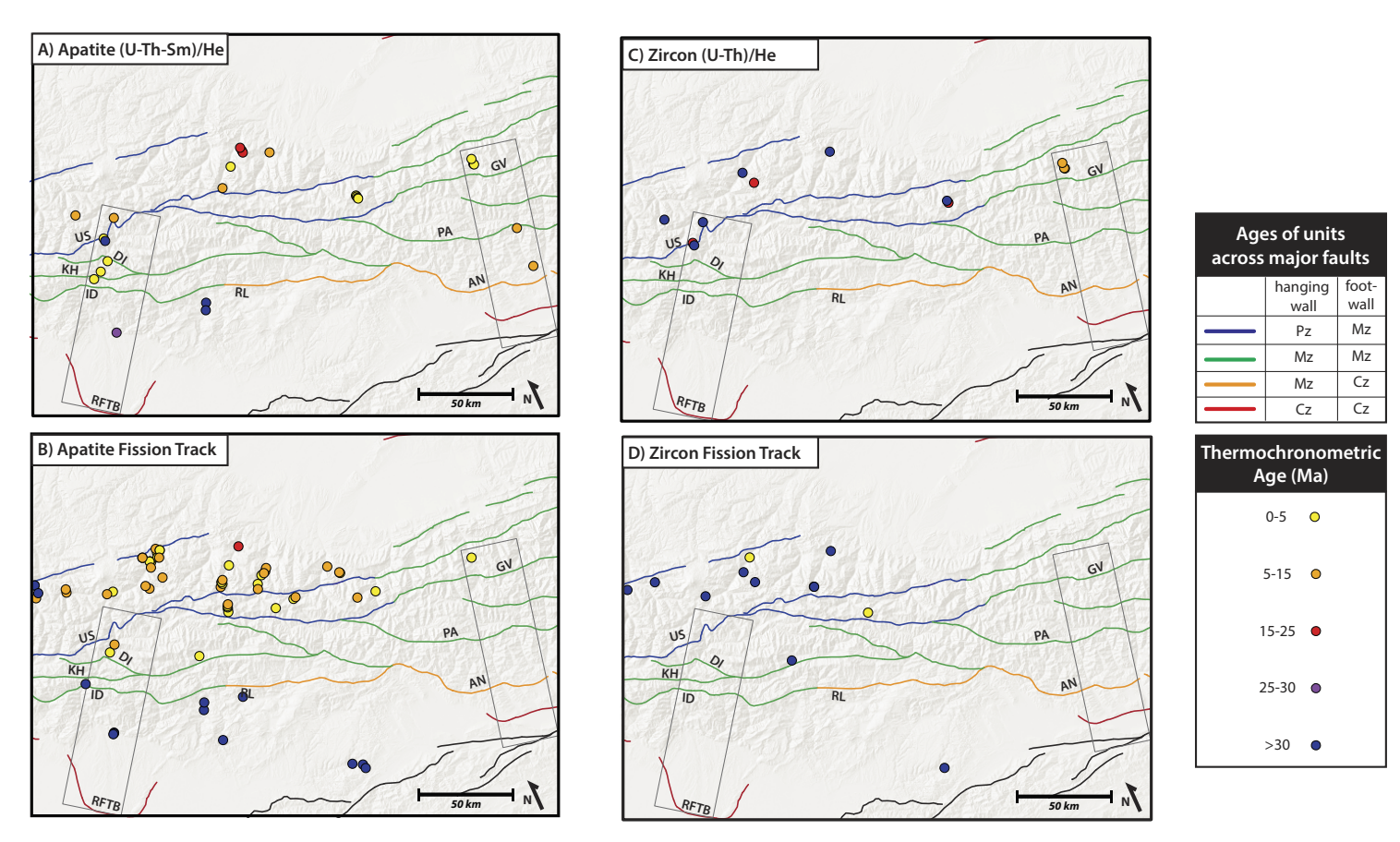


Figure 9. Locations and ages of new and previously published low-temperature thermochronology analyses in the western Greater Caucasus. Data set was compiled from Hess et al. (1993); Kral and Gurbanov (1996); Avdeev (2011); Avdeev and Niemi (2011); Vincent et al. (2011, 2020); and Vasey et al. (2020). (A) Apatite (U-Th-Sm)/He. (B) Apatite fission track. (C) Zircon (U-Th)/He. (D) Zircon fission track. Shades of yellow, orange, and red indicate collisional samples; blue indicates precollisional samples. Map extent is identical to Figure 1B. Faults are colored by relative age juxtaposition across structures. Black lines indicate Lesser Caucasus structures. Faults within the North Georgia fault system are labeled: US - Ushba; DI — Dizi; KH — Khaishi, ID — Idliani; RL — Racha/Lehkhumi; RFTB — Rioni fold-and-thrust belt; GV — Gveleti; PA — Pasanauri; AN — Ananuri. Ages: Pz — Paleozoic; Mz — Mesozoic; Cz — Cenozoic.

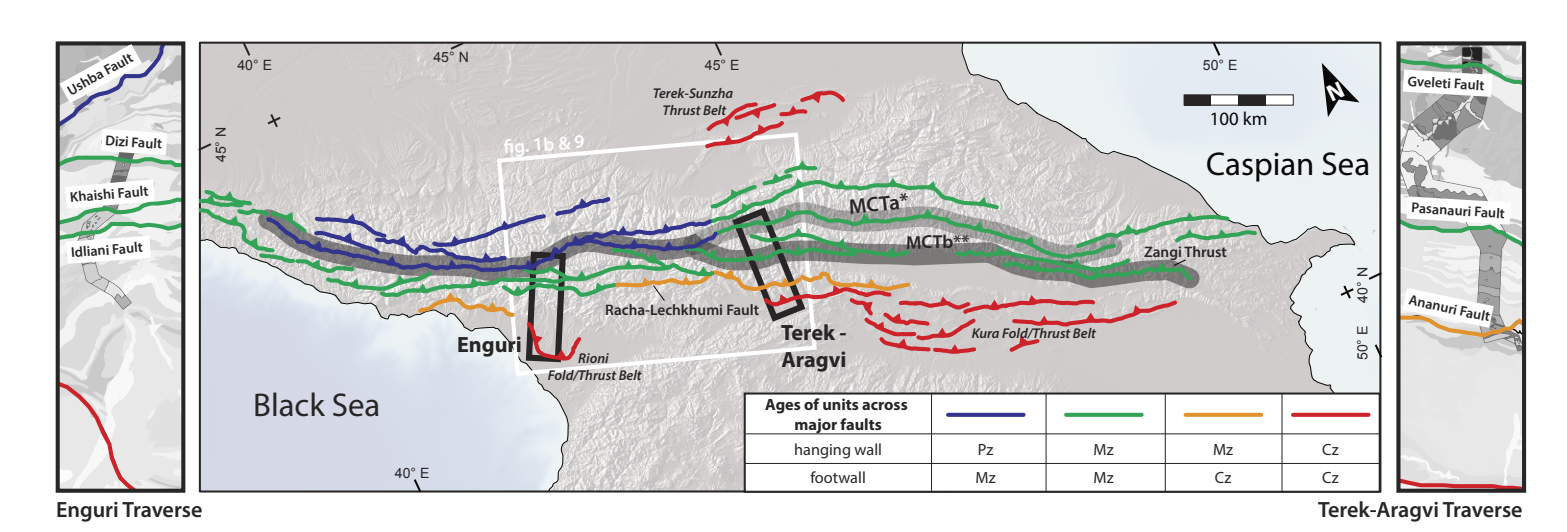


Figure 10. Major, through-going faults (>100 km in length) in the Greater Caucasus, compiled from regional geologic maps (Dzhanelidze and Kandelaki, 1957; Kandelaki, 1957; Zdilashavili, 1957; Gamkrelidze, 1958; Gamkrelidze and Kakhazdze, 1959; Gubkina and Ermakov, 1989) and supported by field data reported here. Faults are colored by relative age juxtaposition across structures. Proposed locations of the Main Caucasus thrust (MCT) are highlighted with gray and labeled MCTa* (Mosar et al., 2010; Adamia et al., 2011b) and MCTb** (Saintot et al., 2006; Kadirov et al., 2012; Forte et al., 2014). Also labeled is the Racha-Lechkhumi fault. Structures in the Lesser Caucasus are not shown. Ages: Pz—Paleozoic; Nz—Mesozoic; Cz—Cenozoic.

Saintot et al., 2006; Somin, 2011; Adamia et al., 2011a, 2011b; Kadirov et al., 2012; Forte et al., 2014; Vasey et al., 2020), often as various proposed locations of the Main Caucasus thrust. Several of the structures within the proposed North Georgia fault system are consistent with these structures, including in the northern core of the range (MCTa in Fig. 10; Mosar et al., 2010; Adamia et al., 2011b) and along the southeastern range front (MCTb in Fig. 10; Saintot et al., 2006; Kadirov et al., 2012; Forte et al., 2014, 2015b). The juxtaposition of strata of broadly similar age across each thrust fault (other than the Ushba and Gveleti faults) suggests that no single primary fault exists along the full strike of the range. Instead, each fault in the North Georgia fault system appears to play a similar role in the construction of the orogen.

The ages of the structures within the North Georgia fault system, as constrained by ages of the units they deform, decrease on the north and south flanks of the range compared to within its core. While this does not preclude young activity on structures in the core of the range, it suggests a structural geometry consistent with the interpretation of the central Greater Caucasus as a bivergent orogenic wedge (Forte et al., 2014). A pattern of structural orientations oblique (<20°) to the strike of the orogen is consistent along strike of the range. This divergence may be due to the original geometry of the Greater Caucasus Basin or subbasins within the greater basin (e.g., Adamia et al., 2011a). Alternatively, we propose that it may result from oblique plate convergence across the Greater Caucasus Basin.

Ushba/Dizi-Gveleti/Pasanauri Fault System

Our field data and structural interpretations lead us to correlate the Ushba/ Dizi faults along the Enguri traverse with the Gveleti/Pasanauri faults along the Terek-Aragvi traverse to create the northernmost fault in the North Georgia fault system. This connection is supported by field data showing consistent bedding and structural orientations and correlation of map units on 1:200,000 scale geologic maps (Dzhanelidze and Kandelaki, 1957; Kandelaki, 1957; Zdilashavili, 1957; Gamkrelidze, 1958; Gamkrelidze and Kakhazdze, 1959; Gubkina and Ermakov, 1989). However, in detail, the internal correlations within the Ushba/Dizi-Gveleti/Pasanauri system are unclear, due to the lack of detailed thermochronologic, lithologic, and provenance observations needed to correlate specific tectonostratigraphic units and their bounding faults within the system. One possibility is that the Ushba fault branches eastward along strike to link with both the Gveleti and Pasanauri faults. Another is that the Ushba and Gveleti faults are linked to one another and are separate from the Dizi and Pasanauri faults, which are connected via a fault not shown on Figure 10. Prior work has argued that the Ushba-Pasanauri structure is an inherited structure that is as old as Middle Jurassic, predating much of the deposition within the Greater Caucasus Basin, and so it does not represent a high-displacement Cenozoic thrust (e.g., Somin, 2011). Recent work by Vasey et al. (2020) documented Mesozoic shearing along the Gveleti and possibly the Ushba shear

zones, which clearly indicates that while these structures accommodated some of the Cenozoic exhumation within the Greater Caucasus, a substantial component of this exhumation was due to slip along other thrusts to the south within the North Georgia fault system.

Khaishi/Idliani-Racha-Lechkhumi-Ananuri Fault System

Based on our field mapping and compilation of map and thermochronologic data, we also suggest an along-strike connection of the Khaishi/Idliani faults on the Enguri traverse with the Ananuri fault at the southern end of the Terek-Aragvi traverse via the intervening Racha-Lechkhumi fault (as defined by Vincent et al., 2018). We further propose that the Khaishi/Idliani–Racha-Lechkhumi–Ananuri fault system links with the Zangi thrust at the southern mountain front in the eastern Greater Caucasus in Azerbaijan, which has been interpreted as the primary shortening structure (MCTb in Fig. 10) in this part of the orogen (Saintot et al., 2006; Forte et al., 2014). Importantly, the Zangi thrust also clearly juxtaposes southern volcaniclastic and northern nonvolcaniclastic domains (Kopp and Shcherba, 1985), similar to the Idliani/Khaishi fault system along the Enguri traverse.

Field observations, combined with initial basin geometry interpreted from detrital zircon provenance data (Cowgill et al., 2016), highlight the significance of the Khaishi/Idliani–Racha–Lechkhumi–Ananuri fault system as a major shortening structure. On the Enguri traverse, field data, including paleoflow directions, correlate well with existing detrital zircon data (Cowgill et al., 2016), suggesting the existence of a major shortening structure in the central part of the traverse, likely along the Khaishi and/or Idliani faults. On the Terek-Aragvi traverse, no detrital zircon provenance data have been reported to constrain the locations of zones of major shortening. Field observations and structural interpretations suggest that the Ananuri fault, at the southern end of the traverse, is likely to be such a major shortening structure, based on the juxtaposition of distinct rock types across this fault and its truncation of a continuous stratigraphic package within the structurally imbricated strata of the Pasanauri domain to the north.

Combining Geological Observations and Low-Temperature Thermochronology

The apatite (U-Th-Sm)/He and fission-track results reported here contribute to a growing data set documenting the exhumation history of the western Greater Caucasus (Kral and Gurbanov, 1996; Avdeev and Niemi, 2011; Vincent et al., 2011, 2020; Vasey et al., 2020). The combined data indicate systematic variations in the depth of exhumation across strike, with low-temperature thermochronometers yielding collisional ages (as defined in the "Evidence from Low-Temperature Thermochronology" subsection of the "Evidence for Major Structures" section) in the core of the range and precollisional ages on the margins, with the regional extent of collisional ages increasing in area

inversely with the closure temperature of the given system, such that the system with the lowest closure temperature, i.e., apatite (U-Th-Sm)/He, has the largest area of collisional ages (Fig. 9; Table S4). Boundaries between domains with collisional and precollisional ages appear to correlate well with structures in the North Georgia fault system (Figs. 9 and 10): The Idliani fault defines the boundary in the apatite (U-Th-Sm)/He system, and the Khaishi fault defines the boundary in the apatite fission-track system. Samples from the hanging wall (north) of the Ushba/Dizi and Gveleti/Pasanauri faults record the deepest exhumation levels in the range. Meanwhile, samples from the footwall (south) of the Khaishi/Idliani-Racha-Lehkhumi-Ananuri fault systematically record ages older than Cenozoic, consistent with limited exhumation in that portion of the orogen. Although samples are limited between the Ushba/Dizi-Gveleti/ Pasanauri faults in the north and the Khaishi/Idliani-Racha-Lehkhumi-Ananuri faults in the south, the existing data record a mixture of collisional apatite (U-Th-Sm)/He and precollisional apatite fission-track ages, suggesting intermediate magnitudes of exhumation.

These results are consistent with the interpretation that structure(s) within the North Georgia fault system represent significant structural boundaries in the orogen. The spatial separation of collisional versus precollisional age boundaries in different thermochronologic systems may additionally have been triggered or amplified by lateral advection of material during exhumation (e.g., Batt and Brandon, 2002), as might be expected in an accretionary prism–like environment. No single structure appears to act as a boundary between dramatically different exhumation magnitudes (i.e., a collocated break in ages of multiple thermochronologic systems), as might be expected if a structure was actively accommodating vertical displacement.

Addressing Prior Structural Interpretations

Main Caucasus Thrust and the North Georgia Fault System

Major structures within the Greater Caucasus are the subjects of various, typically contradictory interpretations regarding their significance and role in the orogen, resulting in the lack of a coherent structural framework. One such major structure is the north-dipping Main Caucasus thrust, which is widely cited as the primary structure of the orogen. However, interpretations of the location, geometry, and significance of the Main Caucasus thrust are highly variable. Some infer that the Main Caucasus thrust is active and accommodates most shortening across the Greater Caucasus (e.g., Philip et al., 1989; Jackson, 1992; Allen et al., 2004; Reilinger et al., 2006). The Main Caucasus thrust has been variably interpreted as a low-angle thrust with >30 km of slip (e.g., Dotduyev, 1986; Mosar et al., 2010), a high-angle fault with minor horizontal displacement (e.g., Somin, 2000, 2011), a remnant of the Paleotethys suture (e.g., Natal'in and Şengör, 2005), and both the basal detachment (Mosar et al., 2010) and backstop (Forte et al., 2014) of a southward-propagating thrust wedge. In addition, the location of the Main Caucasus thrust is disputed, particularly in the eastern

Greater Caucasus, where some authors place it near the southern topographic front of the range (e.g., Saintot et al., 2006; Kadirov et al., 2012; Forte et al., 2014, 2015a), while others place it farther north, near the topographic crest of the range (Mosar et al., 2010; e.g., Adamia et al., 2011b). Low-temperature thermochronology across one of the Main Caucasus thrust candidate faults, in the core of the western Greater Caucasus, suggests that the fault in question may accommodate some component of Cenozoic exhumation, but that other Cenozoic structures to the south are also important (Vasey et al., 2020).

The orogenic architecture we propose here may in part explain the confusion in published literature regarding the location of the Main Caucasus thrust. Rather than a single dominant fault extending the length of the orogen, we instead documented multiple significant structures that appear to be more-orless continuous along strike. We propose that the Ushba/Dizi–Gveleti/Pasanauri and Idliani/Khaishi–Racha/Lehkhumi–Ananuri fault systems are two examples of such continuous structures within the North Georgia fault system, which extends throughout the western Greater Caucasus (Fig. 9).

Each of these structures has the potential to be interpreted as the Main Caucasus thrust in one or more locations along its strike; however, our results suggest that no single surface-breaking fault functions as the primary structure within the orogen. We suggest that by highlighting multiple potentially major structures within the orogen, the North Georgia fault system provides a more productive framework for understanding the structural geometry of the western Greater Caucasus than the current Main Caucasus thrust paradigm.

Role of High-Angle Structures in the Greater Caucasus

Prior studies (e.g., Adamia et al., 2011b; Vincent et al., 2018) have documented multiple high-angle faults in the core of the western Greater Caucasus, including the structures that make up the North Georgia fault system. These faults are often considered to have formed as extensional structures during earlier tectonic episodes and to have been reactivated in the current tectonic setting as reverse faults (Yakovlev, 2012; e.g., Vincent et al., 2018). In this view, and given their steep dips, such structures have been proposed to accommodate rock uplift within the orogen with relatively little shortening.

The observations we present here support an alternative explanation: Namely, these structures did not originally form at high angles but instead initiated as lower-angle thrust faults that have since been rotated to their current orientations by progressive southward propagation of the active thrust front as the orogen has grown. We support this interpretation by noting that while faults within these domains are high-angle structures in their current positions, they appear to be low-angle structures relative to the bedding they crosscut, which is also steeply dipping and even subvertical in the northern tectonostratigraphic domains (Figs. 2 and 6). The lithology across low-angle faults suggests that such structures may record multiple kilometers of displacement, enough to juxtapose units from different depositional facies and exhumation levels, and other spatially and temporally derived lithologic

changes, against each other. Such subparallel bedding and fault orientations are relatively easily produced in a single tectonic setting when the deformation is accommodated in repeated thrust sheets (i.e., an imbricate fan). The alternative model for producing this geometric relationship—that high-angle normal faults formed within a package of already steeply dipping stratigraphy—would require multiple discrete tectonic episodes since the deposition of the Mesozoic-age Caucasus Basin stratigraphic section (compression to deform bedding, followed by extension to form normal faults, and finally compression to reactivate faults as high-angle reverse faults). This multiphase history is not supported by other data sets in the current model of Greater Caucasus evolution (see "Background" section; Fig. 1B).

We did not document discrete, nor significant, change in exhumation magnitude as indicated by metamorphic grade and low-temperature thermochronology across any individual fault, as might be expected if these high-angle structures were active in their current orientation. Instead, exhumation magnitude gradually increases in the interior of the range but does not seem to be concentrated across any individual fault. Additional thermochronology data sets are needed to more conclusively document exhumation patterns across individual structures.

Researchers have debated the existence and relative importance of highangle, often orogen-oblique, strike-slip faults within the Greater Caucasus. We did not observe any field-based evidence for these strike-slip structures, and other published geologic maps (e.g., Dzhanelidze and Kandelaki, 1957; Kandelaki and Kakhazdze, 1957) show no offsets of stratigraphic contacts or faults that would support their existence.

Greater Caucasus as an Imbricate Fan

In sum, we interpret the combined data presented here to indicate that the western Greater Caucasus defines an imbricate fan (e.g., Boyer and Elliott, 1982), with decreasing fault and bedding dips and decreasing exhumation depth from north to south along both traverses (see stereograms, Figs. 2 and 6). The notable exception to this pattern is the Ushba fault on the Enguri traverse, which has a moderate northward dip (~40°N); this structure was inherited from earlier (Mesozoic) orogenic episodes and may not be active in the Cenozoic (Vasey et al., 2020). Elsewhere on both traverses, thrust sheets at the northern ends of the traverses have been lifted and steepened by each successive thrust sheet added to the bottom of the imbricate stack as the active thrust front has propagated southward to its current location at the southern end of the traverses. This progressive, stepwise thrust front propagation and formation of new thrust sheets resulted in oversteepening and local overturning of the previously active thrust sheets-in this case, structures in the northern portion of each traverse, such as the secondary faults north of the Pasanauri fault on the Terek-Aragvi traverse (Fig. 6). This model is consistent with our structural observations along both traverses, which exhibit increasing dip angles from south to north. In this model, the western Greater Caucasus may

thus be analogous to the Triassic Songpan Ganzi complex in Tibet, in which a package of turbidites was shortened into a belt of tight, upright folds with associated metamorphism that was primarily low grade (Roger et al., 2008, 2010; Weislogel, 2008).

As a result of progressive back-rotation, the model predicts that faults within the core of the range will also be steeply dipping or even overturned in the modern orogen, again consistent with our observations. Thus, the model provides an explanation for the high-angle faults observed within the Greater Caucasus core (Somin, 2000; e.g., Adamia et al., 2011b; Vincent et al., 2018) while also allowing for tens of kilometers or more of displacement across these structures at earlier stages of orogen growth. This model is additionally supported by low-temperature thermochronology data, which support progressive increases in exhumation depth from the flanks of the range to its core, but which do not appear to record large magnitudes of exhumation across any individual structure.

Evolution of the Caucasus Basin

The structural, stratigraphic, petrographic, and geochemical observations we present here provide additional insight into the paleogeography of the Caucasus Basin, particularly during the Mesozoic. Much of the sedimentary section exposed within the Greater Caucasus Mountains was deposited within the Mesozoic-age Greater Caucasus Basin (see "Geologic Setting" subsection of the "Background" section; Fig. 1C), which we broadly define as a back-arc extensional basin (or set of basins) related to the subduction of Tethys Ocean to the south of its southern margin (McCann et al., 2010; Mosar et al., 2010). The presence of marine basin sedimentary rocks such as turbidites does not constrain the scale or paleogeography of this basin, because such deposits exhibit runout distances from a few tens to over a thousand kilometers (Mutti et al., 2009). Analysis of detrital zircon provenance data from the Greater Caucasus records minimal depositional exchange across the basin (Cowgill et al., 2016), and Cowgill et al. (2016) suggested a maximum basin width of ~350-400 km based on the widths of the modern Black Sea and South Caspian Basins, which are presumed to be along-strike analogues. Further stratigraphic and structural data are required to better constrain the amount of crustal shortening recorded within the orogen, and thus the scale of the marine basin represented by these units.

Our stratigraphic observations broadly support the interpretations of basin geometry inferred from detrital zircon provenance analysis (Cowgill et al., 2016). On the Enguri traverse, relative grain size of sedimentary units is finest near the southern end of the Khaishi domain, in agreement with the interpretation of this stratigraphy being deposited in the interior and most distal parts of the marine basin between the Paleozoic crystalline rocks to the north and the Lesser Caucasus arc to the south (Fig. 1C). Sedimentary structures suggest flow directions from the north on the northern end of the mapping transect (in units E-ds2 and E-ks) and from the south at the southern end of

the mapping transect (in E-js and E-jv), also suggesting input from sources on both sides of the basin.

Along the Terek-Aragvi traverse, strata in the Pasanauri and Ananuri domains also show consistently south-directed flow. However, south of the Ananuri fault, flow directions appear to shift, with several outcrops of A-js2 containing cross-beds with internally varying flow directions, suggesting local channelization or climbing ripples that may obscure a signal. Importantly, the rocks exposed in the Jinvali domain are not seen elsewhere on the Terek-Aragvi traverse, including massive carbonate and pebble conglomerate. The stratigraphy and sedimentary structures exposed in the Jinvali domain are consistent with prior interpretation of this domain as an imbricated sequence of Eocene olistolith-bearing strata (Banks et al., 1997), and they suggest a different sediment source and depositional setting than units exposed north of the Ananuri fault. Banks et al. (1997) proposed that the strata in this tectonostratigraphic domain are associated with the southern flank of the Greater Caucasus marine basin, while units north of the Ananuri fault represent deposits from within the marine basin.

Our new major- and trace-element geochemical analyses of maficintermediate rocks consistently yielded LREE enrichment and negative Nb-Ta anomalies in the Jurassic volcanic/volcaniclastic section of the Caucasus Basin (Fig. 5). These signatures are comparable with those seen in island-arc basalt (IAB) and are indicative of a melt source influenced by subduction-zone fluids (e.g., Jakes and Gill, 1970; Kelemen et al., 2003). Although most commonly associated with volcanic arcs, the LREE enrichment and negative Nb-Ta anomalies are also predominant in continental back-arc basin settings such as the Bransfield Strait, Okinawa Trough, and Tyrrhenian Sea (e.g., Saunders and Tarney, 1984; Shinjo et al., 1999; Keller et al., 2002; Trua et al., 2014). Thus, our geochemical analyses are consistent with previous workers who interpreted these volcanic rocks to have been emplaced/deposited in a back-arc basin north of, and behind, the Lesser Caucasus arc and above a north-dipping Neotethyan subduction zone (e.g., Zonenshain and Le Pichon, 1986; Saintot et al., 2006; McCann et al., 2010; Vincent et al., 2016; e.g., Fig. 1C). Our analyses do not provide new evidence either supporting or refuting possible back-arc spreading in the Caucasus Basin, which would predict that some samples have the LREE depletion and lack of Nb-Ta anomalies typical of N-MORB sourced from previously depleted asthenosphere (e.g., Saunders and Tarney, 1984; Pearce and Stern, 2006). However, a subset of samples elsewhere in the Caucasus Basin does contain N-MORB-like signatures (Lordkipanidze et al., 1989; McCann et al., 2010), and our analyses are consistent with, if not diagnostic of, Jurassic back-arc spreading in the Caucasus Basin.

Our field observations also help to further develop understanding of the sediment sources feeding the Tertiary foreland basins to the south of the Greater Caucasus. Prior studies have identified high proportions of volcanic lithic fragments in Oligocene–Miocene sandstone deposited in the foreland basins south of the western Greater Caucasus, and they have determined that these sediments were not derived from the Lesser Caucasus to the south (Figs. 1B and 1C) based on the dominance of south-directed paleoflow at the

time of deposition (Vincent et al., 2013, 2014). Instead, these researchers proposed that these sediments were sourced from a volcanic/volcaniclastic-rich "subbasin" that may have existed within the western Greater Caucasus Basin but is no longer exposed. We suggest that the source(s) of these lithic fragments may have been the volcanic/volcaniclastic units E-kv and/or E-jv, which are widely exposed along the Enguri mapping traverse in western Georgia.

In this understanding of the western Greater Caucasus, structure(s) within the North Georgia fault system represent an enigmatic suture between rocks originating from opposite sides of the Mesozoic-aged Greater Caucasus Basin (e.g., Fig. 1C). Any (and perhaps several) of the major faults within the North Georgia fault system may act as significant shortening structures accommodating closure of the Greater Caucasus Basin. Provenance, stratigraphic, and thermochronologic data currently available suggest that the Khaishi/Idliani–Racha–Lechkhumi–Ananuri fault is likely the primary suture, but further work is needed on all structures within the North Georgia fault system to assess this assertion and fully understand the role each structure played in the Cenozoic evolution of the Caucasus orogen.

CONCLUSIONS

Detailed geologic mapping along two traverses across the Greater Caucasus Mountains revealed uniform structural orientations along the orogen and coherent stratigraphy consistent with the interpretation of the Greater Caucasus as the result of closure of a back-arc marine basin (e.g., Adamia et al., 2011a). Structures along both traverses are most simply interpreted as a broadly in-sequence, southward-propagating imbricate thrust fan, with repeating thrust sheets of similar stratigraphy and decreasing dip angle and exhumation depth from north to south (this pattern is particularly well expressed on the Terek-Aragvi traverse in the central Greater Caucasus). The structures themselves generally are shallowly dipping relative to bedding in their hanging walls, suggesting that they originated as low-angle structures, and lithologic facies juxtaposition across faults suggests potentially multiple kilometers of horizontal transport. Taken together, the data we present here are consistent with a model of Greater Caucasus evolution in which the orogen grows through displacement on low-angle thrusts, rather than reactivation of rift-associated high-angle normal faults.

The Greater Caucasus imbricate fan is subdivided by several major structural boundaries along each of our traverses across the western range, which we refer to collectively as the North Georgia fault system. In each case, these structural boundaries are exhibited by stratigraphic juxtaposition and changes in exhumation depth and metamorphic grade. One such fault, the Ushba-Pasanauri fault, is consistent with the location of the Main Caucasus thrust as defined by Adamia et al. (2011b), Mosar et al. (2010), and Vasey et al. (2020) in Georgia. Another fault, the Khaishi/Idliani–Ananuri fault system, appears to correspond with the Racha–Lehkhumi system of Saintot et al. (2006) and Vincent et al. (2018). The presence of multiple significant fault systems within

the range may have contributed to the confusion in the literature around the location of a singular Main Caucasus thrust. We propose that defining these faults collectively as the North Georgia fault system, rather than individually, more accurately represents the structural geometry and kinematics we observed on the ground.

Moreover, we argue that the North Georgia fault system provides an important framework for future investigations into the tectonic evolution of the Greater Caucasus. A fundamental prediction of the continental collision model of Greater Caucasus growth (e.g., Cowgill et al., 2016) is that there must be, somewhere within the western Greater Caucasus, a tectonic suture that marks the transition between material originating on the overriding plate to the north and rocks derived from the downgoing or underthrust plate to the south. We suggest that the North Georgia fault system represents this suture zone, and future work may allow us to determine the kinematics and evolution of individual faults in the system.

ACKNOWLEDGMENTS

This work was supported by research grants to Trexler from the Geological Society of America, the American Association of Petroleum Geologists, the Evolving Earth Foundation, and the Achievement Rewards for College Scientists Foundation. This material is based upon work supported by the National Science Foundation (NSF) under grant numbers 0810285 and 1524631 to Cowgill and 0810067 and 1524304 to Niemi from the EAR-Tectonics program, with support from the Office of International Science and Engineering. Thanks go to George Gehrels, Mark Pecha, and Kojo Plange for assistance with U-Pb analyses at the Arizona LaserChron Center, which is supported by NSF EAR grant 1649254. Matty Mookerjee graciously conducted and interpreted the electron backscatter diffraction (EBSD) analysis. We thank Giorgi Boichenko, Mamuka Natsvilishvili, Salome Gogoladze, and Alex Tye for their invaluable assistance with field work, Amanda Maslyn at the University of Michigan Thermochronology Laboratory for (U-Th)/He analyses, and Greg Baxter at the University of California-Davis for preparing thin sections. Mike Oskin provided valuable feedback on early versions of this manuscript, Ben Melosh, Steve DeLong, Matty Mookeriee, Delores Robinson, an anonymous reviewer, Associate Editor Jeff Lee, and Science Editor Andrea Hampel contributed helpful and constructive reviews. We also thank Adam Forte for his invaluable assistance and advice in the field and throughout the preparation of this manuscript. Any use of trade, firm, or product names is for descriptive purposes only and does not imply endorsement by the U.S. government.

REFERENCES CITED

- Adamia, S., Alania, V., Chabukiani, A., Kutelia, Z., and Sadradze, N., 2011a, Great Caucasus (Cavcasioni): A long-lived north-Tethyan back-arc basin: Turkish Journal of Earth Sciences, v. 20, p. 611–628, https://doi.org/10.3906/yer-1005-12.
- Adamia, S., Zakariadze, G., Chkhotua, T., Sadradze, N., Tsereteli, N., Chabukiani, A., and Gventsadze, A., 2011b, Geology of the Caucasus: A review: Turkish Journal of Earth Sciences, v. 20, p. 489–544, https://doi.org/10.3906/yer-1005-11.
- Adamia, S., Alania, V., Tsereteli, N., Varazanashvili, O., Sadradze, N., Lursmanashvili, N., and Gventsadse, A., 2017, Postcollisional tectonics and seismicity of Georgia, in Sorkhabi, R., ed., Tectonic Evolution, Collision, and Seismicity of Southwest Asia: In Honor of Manuel Barberian's Forty-Five Years of Research Contributions: Geological Society of America Special Paper 525, p. 535–572, https://doi.org/10.1130/2017.2525(17).
- Alania, V.M., Chabukiani, A.O., Chagelishvili, R.L., Enukidze, O.V., Gogrichiani, A., Ramadze, A.N., and Tsereteli, N.S., 2017, Growth structures, piggy-back basins and growth strata of the Georgian part of the Kura foreland fold-thrust belt: Implications for late Alpine kinematic evolution, in Sosson, M., Stephenson, R.A., and Adamia, S.A., eds., Tectonic Evolution of the Eastern Black Sea and Caucasus: Geological Society, London, Special Publication 428, p. 171-185, https://doi.org/10.1144/SP428.5.

- Alania, V., Enukidze, O., Sadradze, N., Boichenko, G., Sadradze, G., Chabukiani, A., Kiria, T., Kvavadze, N., and Gventsadze, A., 2020a, 3D structural model of the Bitsmedi anticline using seismic profiles, Georgia: Bulletin of the Georgian National Academy of Sciences, v. 14, no. 1, p. 61–67.
- Alania, V., Beridze, T., Enukidze, O., Lebanidze, Z., Razmadze, A., Sadradze, N., and Tevzadze, N., 2020b, Structural model of the frontal part of the eastern Achara-Trialeti fold-and-thrust belt: The results of seismic profile interpretation: Bulletin of the Georgian National Academy of Sciences, v. 14, no. 2, p. 62-66.
- Allen, M., Jackson, J., and Walker, R., 2004, Late Cenozoic reorganization of the Arabia-Eurasia collision and the comparison of short-term and long-term deformation rates: Tectonics, v. 23, TC2008, https://doi.org/10.1029/2003TC001530.
- Avdeev, B., 2011, Tectonics of the Greater Caucasus and the Arabia-Eurasia Orogen [Ph.D. thesis]: Ann Arbor, Michigan, University of Michigan, 137 p.
- Avdeev, B., and Niemi, N.A., 2011, Rapid Pliocene exhumation of the central Greater Caucasus constrained by low-temperature thermochronometry: Tectonics, v. 30, TC2009, https://doi.org/10.1029/2010TC002808.
- Banks, C.J., Robinson, A.G., and Williams, M.P., 1997, Structure and regional tectonics of the Achara-Trialet fold belt and the adjacent Rioni and Kartli foreland basins, Republic of Georgia, in Robinson, A.G., ed., Regional and Petroleum Geology of the Black Sea and Surrounding Region: American Association of Petroleum Geologists Memoir 68, p. 331–346, https://doi.org/10.1306/M68612C17.
- Batt, G.E., and Brandon, M.T., 2002, Lateral thinking: 2-D interpretation of thermochronology in convergent orogenic settings: Tectonophysics, v. 349, p. 185–201, https://doi.org/10.1016 /S0040-1951(02)00053-7.
- Boyer, S.E., and Elliott, D., 1982, Thrust systems: American Association of Petroleum Geologists Bulletin, v. 66, p. 1196–1230, https://doi.org/10.1306/03B5A77D-16D1-11D7-8645000102C1865D.
- Cabanis, B., and Thieblemont, D., 1988, La discrimination des tholeiites continentales et des basaltes arriere-arc: Proposition d'un nouveau diagramme, le triangle Th-3xTb-2xTa: Bulletin de la Société Géologique de France, v. IV, p. 927–935, https://doi.org/10.2113/gssgfbull.IV.6.927.
- Cowgill, E., Forte, A.M., Niemi, N., Avdeev, B., Tye, A., Trexler, C., Javakhishvili, Z., Elashvili, M., and Godoladze, T., 2016, Relict basin closure and crustal shortening budgets during continental collision: An example from Caucasus sediment provenance: Tectonics, v. 35, p. 2918–2947, https://doi.org/10.1002/2016TC004295.
- Cowgill, E., Niemi, N.A., Forte, A.M., and Trexler, C.C., 2018, Reply to Comment by Vincent et al.: Tectonics, v. 37, p. 1017–1028, https://doi.org/10.1002/2017TC004793.
- Dotduyev, S.I., 1986, Nappe structure of the Greater Caucasus range: Geotectonics, v. 20, p. 420–430.
 Dzhanelidze, A.I., and Kandelaki, N.A., 1957, Geological Map of the USSR, Caucasus Series Sheet
 K-38-XIII: Moscow, Ministry of Geology and Mineral Protection USSR, scale 1:200,000.
- Farley, K.A., 2000, Helium diffusion from apatite: General behavior as illustrated by Durango fluorapatite: Journal of Geophysical Research: Solid Earth, v. 105, p. 2903–2914, https://doi. org/10.1029/1999JB900348.
- Forte, A.M., Cowgill, E., Bernardin, T., Kreylos, O., and Hamann, B., 2010, Late Cenozoic deformation of the Kura fold-thrust belt, southern Greater Caucasus: Geological Society of America Bulletin, v. 122, p. 465–486, https://doi.org/10.1130/B26464.1.
- Forte, A.M., Cowgill, E., Murtuzayev, I., Kangarli, T., and Stoica, M., 2013, Structural geometries and magnitude of shortening in the eastern Kura fold-thrust belt, Azerbaijan: Implications for the development of the Greater Caucasus Mountains: Tectonics, v. 32, p. 688–717, https:// doi.org/10.1002/tect.20032.
- Forte, A.M., Cowgill, E.S., and Whipple, K.X., 2014, Transition from a singly vergent to a doubly vergent wedge in a young orogen: The Greater Caucasus: Tectonics, v. 33, p. 2077–2101, https://doi.org/10.1002/2014TC003651.
- Forte, A.M., Sumner, D.Y., Cowgill, E., Stoica, M., Murtuzayev, I., Kangarli, T., Elashvili, M., Godoladze, T., and Javakhishvili, Z., 2015a, Late Miocene to Pliocene stratigraphy of the Kura Basin, a subbasin of the South Caspian Basin: Implications for the diachroneity of stage boundaries: Basin Research, v. 27, p. 247–271, https://doi.org/10.1111/bre.12069.
- Forte, A.M., Whipple, K.X., and Cowgill, E., 2015b, Drainage network reveals patterns and history of active deformation in the eastern Greater Caucasus: Geosphere, v. 11, p. 1343–1364, https://doi.org/10.1130/GES01121.1.
- Fretzdorff, S., Worthington, T.J., Haase, K.M., Hékinian, R., Franz, L., Keller, R.A., and Stoffers, P., 2004, Magmatism in the Bransfield basin: Rifting of the South Shetland arc?: Journal of Geophysical Research: Solid Earth, v. 109, B12208, https://doi.org/10.1029/2004JB003046.
- Gamkrelidze, P.D., 1958, Geological Map of the USSR, Caucasus Series Sheet K-38-XXI: Moscow, Ministry of Geology and Mineral Protection USSR, scale 1:200,000.

- Gamkrelidze, P.D., and Kakhazdze, I.R., 1959, Geological Map of the USSR, Caucasus Series Sheet K-38-VII: Moscow, Ministry of Geology and Mineral Protection USSR, scale 1:200,000.
- Gleadow, A.J.W., Duddy, I.R., and Lovering, J.F., 1983, Fission track analysis: A new tool for the evaluation of thermal histories and hydrocarbon potential: APPEA Journal, v. 23, p. 93–102, https://doi.org/10.1071/AJ82009.
- Gubkina, A.N., and Ermakov, V.A., 1989, Geological Map of the USSR, Caucasus Series Sheet K-38-IX: Moscow, USSR Ministry of Geology, scale 1:200,000.
- Hess, J.C., Lippolt, H.J., Gurbanov, A.G., and Michalski, I., 1993, The cooling history of the late Pliocene Eldzhurtinskiy granite (Caucasus, Russia) and the thermochronological potential of grain-size/age relationships: Earth and Planetary Science Letters, v. 117, p. 393–406, https:// doi.org/10.1016/0012-821X[93]90092-N.
- Jackson, J., 1992, Partitioning of strike-slip and convergent motion between Eurasia and Arabia in eastern Turkey and the Caucasus: Journal of Geophysical Research, v. 97, p. 12471–12479, https://doi.org/10.1029/92JB00944.
- Jakes, P., and Gill, J., 1970, Rare earth elements and the island arc tholeitic series: Earth and Planetary Science Letters. v. 9. p. 17–28. https://doi.org/10.1016/0012-821X(70)90018-X.
- Kadirov, F., Floyd, M., Alizadeh, A., Guliev, I., Reilinger, R., Kuleli, S., King, R., and Nafi Toksoz, M., 2012, Kinematics of the eastern Caucasus near Baku, Azerbaijan: Natural Hazards, v. 63, p. 997–1006, https://doi.org/10.1007/s11069-012-0199-0.
- Kandelaki, N.A., 1957, Geological Map of the USSR, Caucasus Series Sheet K-37-XVIII: Moscow, Ministry of Geology and Mineral Protection USSR, scale 1:200,000.
- Kandelaki, D.N., and Kakhazdze, I.R., 1957, Geological Map of the USSR, Caucasus Series Sheet K-38-XV: Moscow, Ministry of Geology and Mineral Protection USSR, scale 1:200,000.
- Kelemen, P.B., Hanghøj, K., and Greene, A.R., 2003, One view of the geochemistry of subduction-related magmatic arcs, with an emphasis on primitive andesite and lower crust, in Holland, H.D., and Turekian, K.K., eds., Treatise on Geochemistry, Volume 3: Amsterdam, Netherlands, Elsevier, p. 1–70, https://doi.org/10.1016/B0-08-043751-6/03035-8.
- Keller, R.A., Fisk, M.R., Smellie, J.L., Strelin, J.A., and Lawver, L.A., 2002, Geochemistry of back arc basin volcanism in Bransfield Strait, Antarctica: Subducted contributions and along-axis variations: Journal of Geophysical Research: Solid Earth, v. 107, p. ECV-4-1–ECV-4-17, https:// doi.org/10.1029/2001JB000444.
- Kopp, M.L., and Shcherba, I.G., 1985, Late Alpine development of the east Caucasus: Geotectonics, v. 19, p. 497–507.
- Kral, J., and Gurbanov, A.G., 1996, Apatite fission track data from the Great Caucasus pre-Alpine basement: Chemie der Erde. v. 56. p. 177–192.
- Lordkipanidze, M.B., Meliksetian, B., and Djarbashian, R., 1989, Mesozoic–Cenozoic magmatic evolution of the Pontian–Crimean–Caucasian region, in Rakús, M., Dercourt, J., Nairn, A.E.M., eds., Evolution of the northern Margin of Tethys: IGCP Project 198: Mémoires de la Société Géologique de France, v. 154, p. 103–124.
- Martí, J., Geyer, A., and Aguirre-Diaz, G., 2013, Origin and evolution of the Deception Island caldera (South Shetland Islands, Antarctica): Bulletin of Volcanology, v. 75, p. 732, https://doi.org/10.1007/s00445-013-0732-3.
- McCann, T., Chalot-Prat, F., and Saintot, A., 2010, The early Mesozoic evolution of the western Greater Caucasus (Russia): Triassic-Jurassic sedimentary and magmatic history, in Sosson, M., Kaymakci, N., Stephenson, R.A., Bergerat, F., and Starostenko, V., eds., Sedimentary Basin Tectonics from the Black Sea and Caucasus to the Arabian Platform: Geological Society, London, Special Publication 340, p. 181–238, https://doi.org/10.1144/sp340.10.
- McDonough, W.F., and Sun, S.-S., 1995, The composition of the Earth: Chemical Geology, v. 120, p. 223–253, https://doi.org/10.1016/0009-2541(94)00140-4.
- Morton, A., Allen, M., Simmons, M., Spathopoulos, F., Still, J., Hinds, D., Ismail-Zadeh, A., and Kroonenberg, S., 2003, Provenance patterns in a neotectonic basin: Pliocene and Quaternary sediment supply to the South Caspian: Basin Research, v. 15, p. 321–337, https://doi.org/10 .1046/j.1365-2117.2003.00208.x.
- Mosar, J., Kangarli, T., Bochud, M., Glasmacher, U.A., Rast, A., Brunet, M.F., and Sosson, M., 2010, Cenozoic-Recent tectonics and uplift in the Greater Caucasus: A perspective from Azerbaijan, in Sosson, M., Kaymakci, N., Stephenson, R.A., Bergerat, F., and Starostenko, V., eds., Sedimentary Basin Tectonics from the Black Sea and Caucasus to the Arabian Platform: Geological Society, London, Special Publication 340, p. 261–280, https://doi.org/10.1144/sp340.12.
- Mutti, E., Bernoulli, D., Lucchi, F.R., and Tinterri, R., 2009, Turbidites and turbidity currents from Alpine 'flysch' to the exploration of continental margins: Sedimentology, v. 56, p. 267–318, https://doi.org/10.1111/j.1365-3091.2008.01019.x.

- Nalivkin, D.V., 1973, The Mediterranean geosyncline, *in* Nalivkin, D.V., ed., Geology of the U.S.S.R. [English translation]: Edinburgh, UK, Oliver and Boyd, p. 578–685.
- Natal'in, B.A., and Şengör, A.M.C., 2005, Late Palaeozoic to Triassic evolution of the Turan and Scythian platforms: The pre-history of the Palaeo-Tethyan closure: Tectonophysics, v. 404, p. 175–202, https://doi.org/10.1016/j.tecto.2005.04.011.
- Niemi, N.A., and Clark, M.K., 2018, Long-term exhumation rates exceed paleoseismic slip rates in the central Santa Monica Mountains, Los Angeles County, California: Geology, v. 46, p. 63–66, https://doi.org/10.1130/G39388.1.
- Nikishin, A.M., Ziegler, P.A., Bolotov, S.N., and Fokin, P.A., 2011, Late Palaeozoic to Cenozoic evolution of the Black Sea—Southern Eastern Europe region: Turkish Journal of Earth Sciences, v. 20, p. 571–634, https://doi.org/10.3906/yer-1005-22.
- Pearce, J.A., and Stern, R.J., 2006, Origin of back-arc basin magmas: Trace element and isotope perspectives, in Christie, D.M., Fisher, C.R., Sang-Mook Lee, S.-M., and Givens, S., eds., Back-Arc Spreading Systems: Geological, Biological, Chemical, and Physical Interactions: American Geophysical Union Geophysical Monograph 166, p. 63–86, https://doi.org/10.1029/166GM06.
- Philip, H., Cisternas, A., Gvishiani, A., and Gorshkov, A., 1989, The Caucasus: An actual example of the initial stages of continental collision: Tectonophysics, v. 161, p. 1–21, https://doi.org /10.1016/0040-1951(89)90297-7.
- Potapenko, Y.Y., 1964, Geological Map of the USSR, Caucasus Series Sheet K-38-I: Moscow, Ministry of Geology and Mineral Protection USSR, scale 1:200,000.
- Reilinger, R., McClusky, S., Vernant, P., Lawrence, S., Ergintav, S., Cakmak, R., Ozener, H., Kadirov, F., Guliev, I. Stepanyan, R. Nadariya, M., Hahubia, G., Mahmoud, Sakr, K., ArRajehi, A., Paradissis, D., Al-Aydrus, A., Prilepin, M., Guseva, T., Evren, E., Dmitrotsa, A., Filikov, S., Gomez, F., Al-Ghazzi, R., and Karam, G., 2006, GPS constraints on continental deformation in the Africa-Arabia-Eurasia continental collision zone and implications for the dynamics of plate interactions: Journal of Geophysical Research: Solid Earth, v. 111, B05411, https://doi.org/10.1029/2005jb004051.
- Reiners, P.W., 2005, Zircon (U-Th)/He thermochronometry: Reviews in Mineralogy and Geochemistry, v. 58, p. 151–179, https://doi.org/10.2138/rmg.2005.58.6.
- Roger, F., Jolivet, M., and Malavieille, J., 2008, Tectonic evolution of the Triassic fold belts of Tibet: Comptes Rendus Geoscience, v. 340, p. 180–189, https://doi.org/10.1016/j.crte.2007.10.014.
- Roger, F., Jolivet, M., and Malavieille, J., 2010, The tectonic evolution of the Songpan-Garzê (north Tibet) and adjacent areas from Proterozoic to present: A synthesis: Journal of Asian Earth Sciences, v. 39, p. 254–269, https://doi.org/10.1016/j.jseaes.2010.03.008.
- Saintot, A., Brunet, M.-F., Yakovlev, F., Sebrier, M., Stephenson, R.A., Ershov, A.V., Chalot-Prat, F., and McCann, T., 2006, The Mesozoic–Cenozoic tectonic evolution of the Greater Caucasus, in Gee, D.G., and Stephenson, R.A., eds., European Lithosphere Dynamics: Geological Society, London, Memoir 32, p. 277–289, https://doi.org/10.1144/GSL.MEM.2006.032.01.16.
- Saunders, A.D., and Tarney, J., 1984, Geochemical characteristics of basaltic volcanism within back-arc basins, in Kokelaar, B.P., and Howells, M.F., eds., Marginal Basin Geology: Volcanic and Associated Sedimentary and Tectonic Processes in Modern and Ancient Marginal Basins: Geological Society, London, Special Publication 16, p. 59–76, https://doi.org/10.1144 /GSL.SP.1984.016.01.05.
- Shinjo, R., Chung, S., Kato, Y., and Kimura, M., 1999, Geochemical and Sr-Nd isotopic characteristics of volcanic rocks from the Okinawa Trough and Ryukyu arc: Implications for the evolution of a young, intracontinental back arc basin: Journal of Geophysical Research: Solid Earth, v. 104, p. 10591–10608, https://doi.org/10.1029/1999JB900040.
- Sobornov, K.O., 1994, Structure and petroleum potential of the Dagestan thrust belt, northeastern Caucasus, Russia: Bulletin of Canadian Petroleum Geology, v. 42, p. 352–364, https://doi.org/10.35767/gscpgbull.42.3.352.
- Sobornov, K.O., 1996, Lateral variations in structural styles of tectonic wedging in the northeastern Caucasus, Russia: Bulletin of Canadian Petroleum Geology, v. 44, p. 385–399, https://doi.org/10.35767/gscpgbull.44.2.385.
- Sokhadze, G., Floyd, M., Godoladze, T., King, R., Cowgill, E.S., Javakhishvili, Z., Hahubia, G., and Reilinger, R., 2018, Active convergence between the Lesser and Greater Caucasus in Georgia: Constraints on the tectonic evolution of the Lesser-Greater Caucasus continental collision: Earth and Planetary Science Letters, v. 481, p. 154–161, https://doi.org/10.1016/j.epsl.2017.10.007.
- Somin, M.L., 2000, Structure of axial zones in the central Caucasus: Doklady Earth Sciences, v. 375A, p. 1371–1374.
- Somin, M.L., 2011, Pre-Jurassic basement of the Greater Caucasus: Brief overview: Turkish Journal of Earth Sciences, v. 20, p. 545–610, https://doi.org/10.3906/yer-1008-6.

- Sun, S.-S., and McDonough, W.F., 1989, Chemical and isotopic systematics of oceanic basalts: Implications for mantle composition and processes, in Saunders, A.D., and Norry, M.J., eds., Magmatism in the Ocean Basins: Geological Society, London, Special Publication 42, p. 313–345, https://doi.org/10.1144/GSL.SP1989.042.01.21.
- Szymanski, E., 2005, Structure and Timing of Thrust and Nappe Development within the Mtkvari River Basin, South Kartli Basin, Republic of Georgia [M.S. thesis]: Boston, Massachusetts, Boston College, 89 p.
- Tagami, T., 2005, Zircon fission-track thermochronology and applications to fault studies: Reviews in Mineralogy and Geochemistry, v. 58, p. 95–122, https://doi.org/10.2138/rmg.2005.58.4.
- Tari, G., Vakhania, D., Tatishvili, G., Mikeladze, V., Gogritchiani, K., Vacharadze, S., Mayer, J., Sheya, C., Siedl, W., Banon, J.J.M., and Trigo Sanchez, J.L., 2018, Stratigraphy, structure and petroleum exploration play types of the Rioni Basin, Georgia, in Simmons, M., Tari, G., and Okay, I., eds., Petroleum Geology of the Black Sea: Geological Society, London, Special Publication 464, p. 403–438. https://doi.org/10.1144/SP464.14.
- Tibaldi, A., Alania, V., Bonali, F.L., Enukidze, O., Tsereteli, N., Kvavadze, N., and Varazanashvili, O., 2017a, Active inversion tectonics, simple shear folding and back-thrusting at Rioni Basin, Georgia: Journal of Structural Geology, v. 96, p. 35–53, https://doi.org/10.1016/j.jsg.2017.01.005.
- Tibaldi, A., Russo, E., Bonali, F.L., Alania, V., Chabukiani, A., Enukidze, O., and Tsereteli, N., 2017b, 3-D anatomy of an active fault-propagation fold: A multidisciplinary case study from Tsaishi, western Caucasus (Georgia): Tectonophysics, v. 717, p. 253–269, https://doi.org/10.1016/j.tecto.2017.08.006.
- Tibaldi, A., Bonali, F., Russo, E., and Mariotto, F., 2018, Structural development and stress evolution of an arcuate fold-and-thrust system, southwestern Greater Caucasus, Republic of Georgia: Journal of Asian Earth Sciences, v. 156, p. 226–245, https://doi.org/10.1016/j.jseaes.2018.01.025.
- Tibaldi, A., Tsereteli, N., Varazanashvili, O., Babayev, G., Barth, A., Mumladze, T., Bonali, F.L., Russo, E., Kadirov, F., Yetirmishli, G. and Kazimova, S., 2020, Active stress field and fault kinematics of the Greater Caucasus: Journal of Asian Earth Sciences, v. 188, https://doi.org/10.1016/j.jseaes.2019.104108.
- Trexler, C.C., Cowgill, E., Spencer, J.Q.G., and Godoladze, T., 2020, Rate of active shortening across the southern thrust front of the Greater Caucasus in western Georgia from kinematic modeling of folded river terraces above a listric thrust: Earth and Planetary Science Letters, v. 544, 116362, https://doi.org/10.1016/j.epsl.2020.116362.
- Trua, T., Marani, M., and Barca, D., 2014, Lower crustal differentiation processes beneath a backarc spreading ridge (Marsili Seamount, southern Tyrrhenian Sea): Lithos, v. 190, p. 349–362, https://doi.org/10.1016/j.lithos.2013.12.014.
- Tsereteli, N., Tibaldi, A., Alania, V., Gventsadse, A., Enukidze, O., Varazanashvili, O., and Muller, B.I.R., 2016, Active tectonics of central-western Caucasus, Georgia: Tectonophysics, v. 691, p. 328–344, https://doi.org/10.1016/j.tecto.2016.10.025.
- Tye, A.R., Niemi, N.A., Safarov, R.T., Kadirov, F.A., and Babayev, G.R., 2021, Sedimentary response to a collision orogeny recorded in detrital zircon provenance of Greater Caucasus foreland basin sediments: Basin Research, v. 33, p. 933–967, https://doi.org/10.1111/bre.12499.
- Vasey, D.A., Cowgill, E., Roeske, S.M., and Niemi, N.A., 2020, Evolution of the Greater Caucasus basement and formation of the Main Caucasus thrust: Tectonics, v. 39, e2019TC005828, https:// doi.org/10.1029/2019TC005828.
- Vasey, D.A., Cowgill, E., and Cooper, K.M., 2021, A preliminary framework for magmatism in modern continental back-arc basins and its application to the Triassic–Jurassic tectonic evolution of the Caucasus: Geochemistry, Geophysics, Geosystems, v. 22, e2020GC009490, https://doi.org/10.1029/2020GC009490.
- Vermeesch, P., 2012, On the visualisation of detrital age distributions: Chemical Geology, v. 312, p. 190–194, https://doi.org/10.1016/j.chemgeo.2012.04.021.
- Vincent, S.J., Morton, A.C., Carter, A., Gibbs, S., and Barbadze, T.G., 2007, Oligocene uplift of the western Greater Caucasus: An effect of initial Arabia-Eurasia collision: Terra Nova, v. 19, p. 160–166, https://doi.org/10.1111/j.1365-3121.2007.00731.x.
- Vincent, S.J., Carter, A., Lavrishchev, V., Rice, S.P., and Barabadze, T.G., 2011, The exhumation of the western Greater Caucasus: Geological Magazine, v. 148, p. 1–21, https://doi.org/10.1017 /S0016756810000257.
- Vincent, S.J., Morton, A.C., Hyden, F., and Fanning, M., 2013, Insights from petrography, mineralogy and U-Pb zircon geochronology into the provenance and reservoir potential of Cenozoic siliciclastic depositional systems supplying the northern margin of the eastern Black Sea: Marine and Petroleum Geology, v. 45, p. 331–348, https://doi.org/10.1016/j.marpetgeo.2013.04.002.
- Vincent, S.J., Hyden, F., and Braham, W., 2014, Along-strike variations in the composition of sandstones derived from the uplifting western Greater Caucasus: Causes and implications

- for reservoir quality prediction in the eastern Black Sea, in Scott, R.A., Smyth, H.R., Morton, A.C., and Richardson, N., eds., Sediment Provenance Studies in Hydrocarbon Exploration and Production: Geological Society, London, Special Publication 386, p. 111–127, https://doi.org/10.1144/SP386.15.
- Vincent, S.J., Braham, W., Lavrishchev, V.A., Maynard, J.R., and Harland, M., 2016, The formation and inversion of the western Greater Caucasus Basin and the uplift of the western Greater Caucasus: Implications for the wider Black Sea region: Tectonics, v. 35, p. 2948–2962, https:// doi.org/10.1002/2016TC004204.
- Vincent, S.J., Saintot, A., Mosar, J., Okay, A.I., and Nikishin, A.M., 2018, Comment on "Relict basin closure and crustal shortening budgets during continental collision: An example from Caucasus sediment provenance" by Cowgill et al. (2016): Tectonics, v. 37, p. 1006–1016, https:// doi.org/10.1002/2017TC004515.
- Vincent, S.J., Somin, M.L., Carter, A., Vezzoli, G., Fox, M., and Vautravers, B., 2020, Testing models of Cenozoic exhumation in the western Greater Caucasus: Tectonics, v. 39, e2018TC005451, https://doi.org/10.1029/2018TC005451.
- Weislogel, A.L., 2008, Tectonostratigraphic and geochronologic constraints on evolution of the northeast Paleotethys from the Songpan-Ganzi complex, central China: Tectonophysics, v. 451, p. 331–345, https://doi.org/10.1016/j.tecto.2007.11.053.

- Yakovlev, F.L., 2012, Identification of geodynamic setting and of folding formation mechanisms using a strain ellipsoid concept for multi-scale structures of the Greater Caucasus: Tectonophysics, v. 581, p. 93–113, https://doi.org/10.1016/j.tecto.2012.06.004.
- Yilmaz, A., Adamia, S., Chabukiani, A., Chkhotua, T., ErdoGan, K., Tuzcu, S. and KarabiyikoĞlu, M., 2000, Structural correlation of the southern Transcaucasus (Georgia)-eastern Pontides (Turkey), in Bozkurt, E., Winchester, J. and Piper. J., eds., Tectonics and Magmatism in Turkey and the Surrounding Area: Geological Society, London, Special Publications, v. 173, p. 171–182, https://doi.org/10.1144/GSL.SP.2000.173.01.08.
- Zakariadze, G.S., Dilek, Y., Adamia, S.A., Oberhänsli, R.E., Karpenko, S.F., Bazylev, B.A., and Solov'eva, N., 2007, Geochemistry and geochronology of the Neoproterozoic Pan-African Transcaucasian Massif (Republic of Georgia) and implications for island arc evolution of the late Precambrian Arabian-Nubian Shield: Gondwana Research, v. 11, p. 92–108, https:// doi.org/10.1016/j.gr.2006.05.012.
- Zdilashavili, V.Y., 1957, Geological Map of the USSR, Caucasus Series Sheet K-37-XII: Moscow, Ministry of Geology and Mineral Protection USSR, scale 1:200,000.
- Zonenshain, L.P., and Le Pichon, X., 1986, Deep basins of the Black Sea and Caspian Sea as remnants of Mesozoic back-arc basins: Tectonophysics, v. 123, p. 181–211, https://doi.org/10.1016/0040-1951(86)90197-6.